Article

Solid-State ^{63}Cu and ^{65}Cu NMR Spectroscopy of Inorganic and Organometallic Copper(I) Complexes

Joel A. Tang, Bobby D. Ellis, Timothy H. Warren, John V. Hanna, Charles L. B. Macdonald, and Robert W. Schurko

J. Am. Chem. Soc., **2007**, 129 (43), 13049-13065• DOI: 10.1021/ja073238x • Publication Date (Web): 09 October 2007

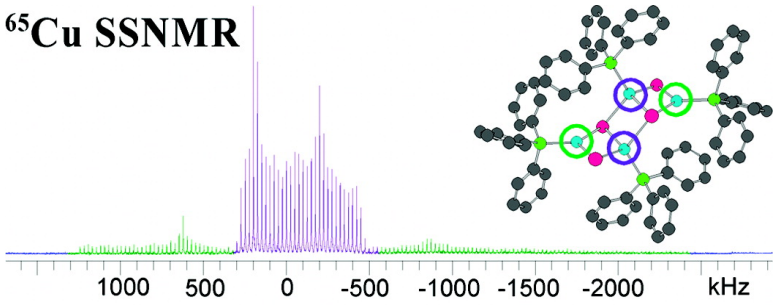

More About This Article

Additional resources and features associated with this article are available within the HTML version:

- Supporting Information
- Links to the 7 articles that cite this article, as of the time of this article download
- Access to high resolution figures
- Links to articles and content related to this article
- Copyright permission to reproduce figures and/or text from this article

View the Full Text HTML

J|A|C|S
ARTICLES
Published on Web 10/09/2007

Solid-State ^{63}Cu and ^{65}Cu NMR Spectroscopy of Inorganic and Organometallic Copper(I) Complexes

Joel A. Tang,[†] Bobby D. Ellis,[†] Timothy H. Warren,[‡] John V. Hanna,[§] Charles L. B. Macdonald,[†] and Robert W. Schurko[†,*]

Contribution from the Department of Chemistry and Biochemistry, University of Windsor, Windsor, Ontario, Canada N9B 3P4, Department of Chemistry, Georgetown University, P.O Box 571227, Washington, D.C. 20057-1227, and ANSTO NMR Facility, Materials Division, Australian Nuclear Science and Technology Organisation, Sydney, Australia, NSW, 2234

Received May 17, 2007; E-mail: rschurko@uwindsor.ca

Abstract: Solid-state ^{63}Cu and ^{65}Cu NMR experiments have been conducted on a series of inorganic and organometallic copper(I) complexes possessing a variety of spherically asymmetric two-, three-, and four-coordinate Cu coordination environments. Variations in structure and symmetry, and corresponding changes in the electric field gradient (EFG) tensors, yield $^{63/65}$Cu quadrupolar coupling constants (C_Q) ranging from 22.0 to 71.0 MHz for spherically asymmetric Cu sites. These large quadrupolar interactions result in spectra featuring quadrupolar-dominated central transition patterns with breadths ranging from 760 kHz to 6.7 MHz. Accordingly, Hahn-echo and/or QCPMG pulse sequences were applied in a frequency-stepped manner to rapidly acquire high *S*/*N* powder patterns. Significant copper chemical shielding anisotropies (CSAs) are also observed in some cases, ranging from 1000 to 1500 ppm. ^{31}P CP/MAS NMR spectra for complexes featuring $^{63/65}$Cu-^{31}P spin pairs exhibit residual dipolar coupling and are simulated to determine both the sign of C_Q and the EFG tensor orientations relative to the Cu−P bond axes. X-ray crystallographic data and theoretical (Hartree−Fock and density functional theory) calculations of $^{63/65}$Cu EFG and CS tensors are utilized to examine the relationships between NMR interaction tensor parameters, the magnitudes and orientations of the principal components, and molecular structure and symmetry.

Introduction

Solid-state copper NMR spectroscopy has been under-utilized for the structural characterization of copper(I) sites in solid materials, primarily because of the large nuclear quadrupole moments of ^{63}Cu and ^{65}Cu nuclei. This is unfortunate, since copper NMR would enhance the currently limited understanding of structure, dynamics, and reactivity at copper(I) sites for many important inorganic materials, organometallic molecules, and biological systems.[1−3] Solid-state copper NMR has largely been applied to Cu sites of high spherical symmetry with reduced electric field gradients (EFGs) and correspondingly small quadrupolar interactions.[4−13] For materials with increasingly spherically asymmetric copper sites, time-consuming wide-line static NMR experiments (i.e., stationary NMR samples) tend to be the norm. For instance, Bastow and co-workers have used static ^{63}Cu NMR experiments to investigate the structural evolution of copper-containing alloys at various temperatures,[8,14] and Antzukin et al. have applied static ^{65}Cu NMR experiments to probe copper environments in a series of copper(I) dialkyldithiophosphate clusters.[15−18] Given the enormous success of NMR of metals for structural characterization, it would greatly benefit chemists, structural biologists, and materials scientists alike to be able to routinely use solid-state copper NMR for characterizing the electronic structure and bonding at Cu(I) sites in systems such as copper proteins,[19−22] amyloid fibrils and related peptides,[23−25] zeolites,[26] organometallic copper com-

[†] University of Windsor.
[‡] Georgetown University.
[§] Australian Nuclear Science and Technology Organisation.

(1) Cotton, F. A.; Wilkinson, G. *Advanced Inorganic Chemistry*, 5th ed.; Wiley: New York, 1988.
(2) Lipshutz, B. H.; Wood, M. R. Copper: Organometallic Chemistry. In *Encyclopedia of Inorganic Chemistry*; King, R. B., Ed.; Wiley: New York 1995, Vol. 2, pp 840.
(3) Conry, R. R.; Karlin, K. D. Copper: Inorganic and Coordination Chemistry. In *Encyclopedia of Inorganic Chemistry*; King, R. B., Ed.; Wiley: New York, 1995, Vol. 2, pp 829.
(4) Yamamoto, T.; Haraguch, H.; Fujiwara, S. *J. Phys. Chem.* **1970**, *74*, 4369.
(5) Kroneck, P.; Lutz, O.; Nolle, A.; Oehler, H. *Z. Naturforsch., A: Phys. Sci.* **1980**, *35*, 221.
(6) Kroeker, S.; Wasylishen, R. E.; Hanna, J. V. *J. Am. Chem. Soc.* **1999**, *121*, 1582.
(7) Liu, H. M.; Sullivan, R. M.; Hanson, J. C.; Grey, C. P.; Martin, J. D. *J. Am. Chem. Soc.* **2001**, *123*, 7564.
(8) Bastow, T. J.; Celotto, S. *Acta Mater.* **2003**, *51*, 4621.
(9) Brunklaus, G.; Chan, J. C. C.; Eckert, H.; Reiser, S.; Nilges, T.; Pfitzner, A. *Phys. Chem. Chem. Phys.* **2003**, *5*, 3768.
(10) Kroeker, S.; Wasylishen, R. E. *Can. J. Chem.* **1999**, *77*, 1962.
(11) Hayashi, S.; Hayamizu, K. *J. Chem. Phys.* **1990**, *92*, 2818.
(12) Hayashi, S.; Hayamizu, K. *J. Phys. Chem. Solids* **1992**, *53*, 239.
(13) Sakida, S.; Kato, N.; Kawamoto, Y. *Mater. Res. Bull.* **2002**, *37*, 2263.
(14) Bastow, T. J.; Celotto, S. *Mater. Sci. Eng., C* **2003**, *23*, 757.
(15) Rusanova, D.; Forsling, W.; Antzutkin, O. N. *Langmuir* **2005**, *21*, 4420.
(16) Rusanova, D.; Forsling, W.; Antzutkin, O. N.; Pike, K. J.; Dupree, R. *J. Mag. Res.* **2006**, *179*, 140.
(17) Rusanova, D.; Pike, K. J.; Dupree, R.; Hanna, J. V.; Antzutkin, O. N.; Persson, I.; Forsling, W. *Inorg. Chim. Acta* **2006**, *359*, 3903.
(18) Rusanova, D.; Pike, K. J.; Persson, I.; Hanna, J. V.; Dupree, R.; Forsling, W.; Antzutkin, O. N. *Chem.—Eur. J.* **2006**, *12*, 5282.
(19) Nersissian, A. M.; Shipp, E. L. Blue copper-binding domains. In *Copper-Containing Proteins*; Academic Press: San Diego, CA, 2002; Vol. 60, pp 271.

plexes,[2] and a wide array of materials where the Cu oxidation state varies or multiple oxidation states simultaneously exist, such as in high-temperature superconductors.[27−30]

The two NMR active isotopes, ^{63}Cu and ^{65}Cu, (both $I = {}^3/_2$) have natural abundances of 69.1% and 30.9%, gyromagnetic ratios (γ) of 7.1088×10^7 and 7.6104×10^7 rad T^{-1} s^{-1}, and nuclear quadrupole moments of -0.220×10^{-28} and -0.204×10^{-28} m^2, respectively.[31] Despite their high receptivities with respect to ^{13}C ($D^C(^{63}\text{Cu}) = 382$ and $D^C(^{65}\text{Cu}) = 208$),[32] the large quadrupolar interactions have largely prohibited routine NMR experimentation, since the central transition powder patterns can be on the order of MHz in breadth. Although ^{63}Cu is more receptive, ^{65}Cu is normally chosen for solid-state NMR experiments owing to its smaller quadrupole moment and higher γ, which serve to reduce the breadth of the large central transition powder patterns.

Copper sites of low symmetry with large quadrupolar interactions have chiefly been characterized with nuclear quadrupolar resonance (NQR). NQR has been used to probe copper sites in inorganic salts,[6] copper halides,[33−37] high-temperature superconductors,[38−41] and magnetic materials.[42−45] While routine NQR experiments can provide extremely accurate measurements of the quadrupolar coupling constant (C_Q), the asymmetry parameter (η_Q) is only accessible through technically demanding, two-dimensional NQR experiments.[46,47] An alternative means of obtaining $C_Q(^{63}\text{Cu})$ and $C_Q(^{65}\text{Cu})$ is via measurements of residual dipolar couplings observed in the spectra of spin-$^1/_2$ nuclei (e.g., ^{31}P) which are dipolar and indirect spin−spin coupled to ^{63}Cu and ^{65}Cu nuclei.[48] This methodology has been used for a variety of spin-$^1/_2$/quadrupolar spin pairs;[48−52] however, there are often large errors associated with the extracted quadrupolar parameters owing to the relative insensitivity of the residual dipolar splittings to changes in C_Q, η_Q, EFG tensor orientation, and the spin−spin coupling parameters. Ideally, if both the spin-$^1/_2$ and quadrupolar NMR spectra can be measured, it is possible to obtain accurate information on the orientation of the EFG tensor in the molecular frame, as well as the sign of C_Q.[10]

The need for rapid and accurate acquisition of wide-line NMR spectra has resulted in the development of frequency-stepped NMR techniques. Traditional frequency-stepped wide-line NMR spectroscopy involves moving the transmitter frequency in evenly spaced increments across a broad range of frequencies and plotting the amplitudes of the Fourier transformed spin−echo as a function of transmitter frequency.[53−58] Co-addition of the piecewise-collected Fourier-transformed spin-echoes is a much more efficient means of producing a uniformly excited powder pattern, owing to a reduction in the number of experiments required.[59,60] However, since such powder patterns are spread out over large frequency ranges, the signal-to-noise ratios (S/N) are inherently low, making this technique time-consuming and generally inapplicable to all but the most receptive nuclei. Recently, the quadrupolar Carr−Purcell Meiboom−Gill (QCPMG) pulse sequence was reintroduced for the acquisition of broad quadrupolar powder patterns of unreceptive nuclei,[61,62] and combined with frequency-stepped wide-line techniques.[56,61,63] This method is ideal for the acquisition of high S/N ^{63}Cu and ^{65}Cu NMR wide-line spectra, permitting characterization of copper sites that were previously unobservable.

Herein we demonstrate that (i) $^{63/65}$Cu NMR spectra can be rapidly acquired for a variety of systems with large quadrupolar interactions and (ii) copper EFG and chemical shielding (CS) tensors are excellent probes of bonding and symmetry at copper sites of varying coordination geometries. We report the application of frequency-stepped $^{63/65}$Cu solid-state NMR experiments to a series of copper(I) compounds which include copper−phosphine metallocenes and a series of coordination complexes with copper in spherically asymmetric two-, three-, and four-coordinate environments (Chart 1). The variety of coordination

(20) Banci, L.; Pierattelli, R.; Vila, A. J. Nuclear magnetic resonance spectroscopy studies on copper proteins. In *Copper-Containing Proteins* Academic Press: San Diego, CA, 2002; Vol. 60, pp 397.
(21) Baker, E. N. Copper Proteins with Type 1 Sites. In *Encyclopedia of Inorganic Chemistry*; King, R. B., Ed.; Wiley: New York, 1995; Vol. 2, pp 883.
(22) McMillin, D. R.; Peyratout, C.; Miller, C. Copper Proteins: Oxidases. In *Encyclopedia of Inorganic Chemistry*; King, R. B., Ed.; Wiley: New York 1995, Vol. 2, pp 869.
(23) Huang, X. D.; et al. *J. Biol. Chem.* **1999**, *274*, 37111.
(24) Cherny, R. A.; et al. *Neuron* **2001**, *30*, 665.
(25) Strange, R. W.; Antonyuk, S.; Hough, M. A.; Doucette, P. A.; Rodriguez, J. A.; Hart, P. J.; Hayward, L. J.; Valentine, J. S.; Hasnain, S. S. *J. Mol. Biol.* **2003**, *328*, 877.
(26) Aylor, A. W.; Larsen, S. C.; Reimer, J. A.; Bell, A. T. *J. Catal.* **1995**, *157*, 592.
(27) Naimushina, Y. A.; Shabanova, I. N.; Chirkov, A. G. *J. Electron Spectrosc. Relat. Phenom.* **2004**, *137−40*, 535.
(28) Luetgemeier, H. *Hyperfine Interact.* **1990**, *61*, 1051.
(29) Geballe, T. H. *J. Supercond. Novel Magn.* **2006**, *19*, 261.
(30) Kivelson, S. A.; Bindloss, I. P.; Fradkin, E.; Oganesyan, V.; Tranquada, J. M.; Kapitulnik, A.; Howald, C. *Rev. Mod. Phys.* **2003**, *75*, 1201.
(31) Pyykko, P. *Mol. Phys.* **2001**, *99*, 1617.
(32) Harris, R. K.; Becker, E. D.; De Menezes, S. M. C.; Goodfellow, R.; Granger, P. *Pure Appl. Chem.* **2001**, *73*, 1795.
(33) Bastow, T. J.; Whitfield, H. J. *J. Mol. Struct.* **1980**, *58*, 305.
(34) Okuda, T.; Hiura, M.; Yamada, K.; Negita, H. *Chem. Lett.* **1977**, 367.
(35) Ramaprabhu, S.; Amstutz, N.; Lucken, E. A. C. *Z. Naturforsch., A: Phys. Sci.* **1994**, *49*, 199.
(36) Ramaprabhu, S.; Lucken, E. A. C.; Bernardinelli, G. *J. Chem. Soc., Dalton Trans.* **1995**, 115.
(37) Lucken, E. A. C. *Z. Naturforsch., A: Phys. Sci.* **1994**, *49*, 155.
(38) Nakamura, Y.; Kumagai, K. *Physica C* **1989**, *162−164*, 187.
(39) Itoh, M.; Karashima, K.; Kyogoku, M.; Aoki, I. *Physica C* **1989**, *160*, 177.
(40) Shimizu, T. *J. Phys. Soc. Jpn.* **1993**, *62*, 779.
(41) Shimizu, T.; Yasuoka, H.; Imai, T.; Tsuda, T.; Takabatake, T.; Nakazawa, Y.; Ishikawa, M. *J. Phys. Soc. Jpn.* **1988**, *57*, 2494.
(42) Young, B.-L.; Curro, N. J.; Sidorov, V. A.; Thompson, J. D.; Sarrao, J. L. *Phys. Rev. B* **2005**, *71*, 224106/1.
(43) Walstedt, R. E.; Kojima, H.; Butch, N.; Bernhoeft, N. *Phys. Rev. Lett.* **2003**, *90*, 067601/1.
(44) Carretta, P.; Sala, R.; Tedoldi, F.; Borsa, F.; Rigamonti, A. *Nuovo Cimento Soc. Ital. Fis., D* **1997**, *19*, 1193.
(45) Itoh, M.; Sugahara, M.; Yamauchi, T.; Ueda, Y. *Phys. Rev. B: Condens. Matter* **1996**, *54*, R9631.
(46) Harbison, G. S.; Slokenbergs, A.; Barbara, T. M. *J. Chem. Phys.* **1989**, *90*, 5292.
(47) Harbison, G. S.; Slokenbergs, A. *Z. Naturforsch., A: Phys. Sci.* **1990**, *45*, 575.
(48) Harris, R. K.; Olivieri, A. C. *Prog. Nucl. Magn. Reson. Spectrosc.* **1992**, *24*, 435.
(49) Olivieri, A. *J. Am. Chem. Soc.* **1992**, *114*, 5758.
(50) Alarcon, S. H.; Olivieri, A. C.; Carss, S. A.; Harris, R. K. *Angew. Chem., Int. Ed.* **1994**, *33*, 1624.
(51) Du, L. S.; Schurko, R. W.; Lim, K. H.; Grey, C. P. *J. Phys. Chem. A* **2001**, *105*, 760.
(52) Schurko, R. W.; Wasylishen, R. E.; Moore, S. J.; Marzilli, L. G.; Nelson, J. H. *Can. J. Chem.* **1999**, *77*, 1973.
(53) Kennedy, M. A.; Vold, R. L.; Vold, R. R. *J. Magn. Res.* **1991**, *92*, 320.
(54) Bastow, T. J. *Z. Naturforsch., A: Phys. Sci.* **1994**, *49*, 320.
(55) Bastow, T. J.; Smith, M. E. *Solid State Nucl. Magn. Reson.* **1992**, *1*, 165.
(56) Lipton, A. S.; Wright, T. A.; Bowman, M. K.; Reger, D. L.; Ellis, P. D. *J. Am. Chem. Soc.* **2002**, *124*, 5850.
(57) Sparks, S. W.; Ellis, P. D. *J. Am. Chem. Soc.* **1986**, *108*, 3215.
(58) Rhodes, H. E.; Wang, P. K.; Stokes, H. T.; Slichter, C. P.; Sinfelt, J. H. *Phys. Rev. B* **1982**, *26*, 3559. We note that in much of Slichter's work on Pt NMR the frequency is held fixed and the field is swept incrementally.
(59) Medek, A.; Frydman, V.; Frydman, L. *J. Phys. Chem. A* **1999**, *103*, 4830.
(60) Massiot, D.; Farnan, I.; Gautier, N.; Trumeau, D.; Trokiner, A.; Coutures, J. P. *Solid State Nucl. Magn. Reson.* **1995**, *4*, 241.
(61) Larsen, F. H.; Jakobsen, H. J.; Ellis, P. D.; Nielsen, N. C. *J. Phys. Chem. A* **1997**, *101*, 8597.
(62) Bryant, P. L.; Butler, L. G.; Reyes, A. P.; Kuhns, P. *Solid State Nucl. Magn. Reson.* **2000**, *16*, 63.
(63) Tang, J. A.; Masuda, J. D.; Boyle, T. J.; Schurko, R. W. *Chem. Phys. Chem.* **2006**, *7*, 117.

Chart 1. Molecular Structures of Compounds Used in this Study[a]

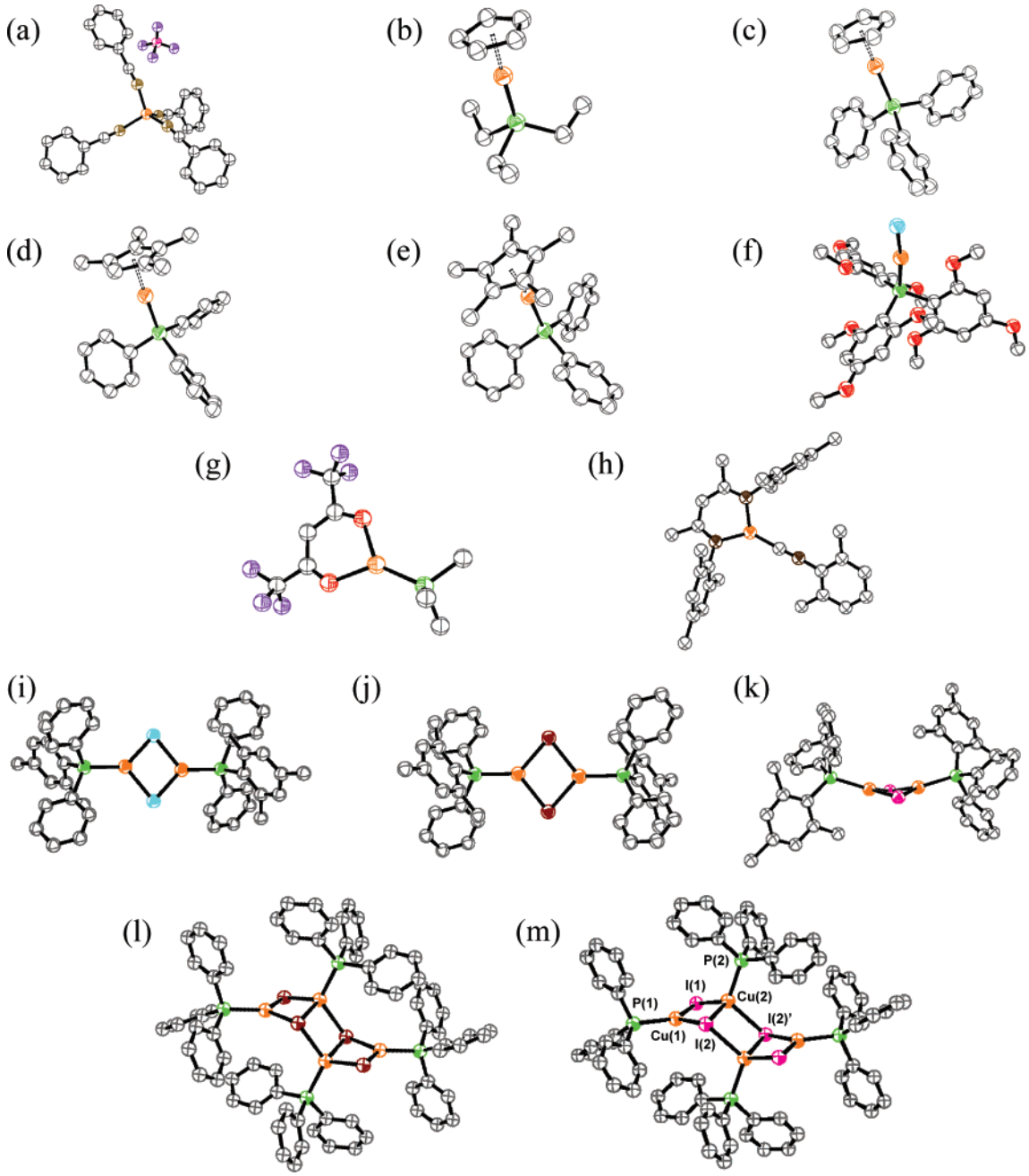

[a] Names and formulas: (a) tetrakisbenzonitrile copper(I) tetrafluoroborate ($[Cu(PhCN)_4]BF_4$), (b) cyclopentadienyl copper(I) triethylphosphine ($CpCuPEt_3$), (c) cyclopentadienyl copper(I) triphenylphosphine ($CpCuPPh_3$), (d) tetramethylcyclopentadienyl copper(I) triphenylphosphine ($Cp^{\dagger}CuPPh_3$), (e) pentamethylcyclopentadienyl copper(I) triphenylphosphine (Cp^*CuPPh_3), (f) tris(2,4,6-methoxyphenyl)phosphinecopper(I) chloride ($ClCuP(2,4,6)_3$), (g) trimethylphosphine(hexafluoroacetylacetonato)copper(I) ((hfac)$CuPMe_3$), (h) β-diketiminato copper(I) isocyanide ($[Me_3NN]Cu(CNAr)$, Ar = 2,6-$Me_2C_6H_3$), (i) bis((mesityldiphenylphosphine)-(μ^2-chloro)-copper(I)) ($[ClCuPPh_2Mes]_2$), (j) bis((mesityldiphenylphosphine)-(μ^2-bromo)-copper(I)) ($[BrCuPPh_2Mes]_2$), (k) bis((mesityldiphenylphosphine)-(μ^2-iodo)-copper(I)) ($[ICuPPh_2Mes]_2$), and stepped clusters (l) tetrameric triphenylphosphine copper(I) bromide ($[BrCuPPh_3]_4 \cdot 2CHCl_3$) and (m) tetrameric triphenylphosphine copper(I) iodide ($[ICuPPh_3]_4$).

environments and molecular symmetries are reflected in the distinct sets of quadrupolar and chemical shift parameters which are extracted via analytical and/or numerical simulations of the copper NMR spectra. Quadrupolar parameters obtained from copper NQR experiments are also reported in select cases. ^{31}P CP/MAS NMR experiments are also reported for the copper phosphine compounds and utilized to experimentally determine both the sign of C_Q and the orientations of the copper EFG tensors with respect to the Cu−P bond axes. In addition, a series of first principles calculations of copper EFG and CS tensors are presented, with the aim of examining relationships between NMR parameters, tensor orientations, and copper environments.

Experimental

Sample Preparation. All reactions were carried out using standard inert-atmosphere techniques. $CpCuPEt_3$, (hfac)$CuPMe_3$ and triphenylphosphine were purchased from Strem Chemicals Inc., and all other chemicals and reagents were obtained from Aldrich. $CpCuPEt_3$ was recrystallized from slow evaporation of pentane, and all other reagents were used without further purification. Solvents were dried on a series

of Grubbs' type columns[64] and were degassed prior to use. Solution NMR spectra were recorded at room temperature in C_6D_6 solutions on a Bruker Advance 300 MHz spectrometer. Chemical shifts are reported in ppm, relative to external standards ($SiMe_4$ for ^1H and ^{13}C, 85% aq H_3PO_4 for ^{31}P). Details on the syntheses of $Cp^{\dagger}CuPPh_3$ and Cp^*CuPPh_3 are given in the Supporting Information.[65] $[Cu(PhCN)_4]BF_4$, $CpCuPPh_3$, $ClCuP(2,4,6)_3$, $[Me_3NN]Cu(CNAr)$, $[ClCuPPh_2Mes]_2$, $[BrCuPPh_2Mes]_2$, $[ICuPPh_2Mes]_2$, $[BrCuPPh_3]_4 \cdot 2CHCl_3$, and $[ICuPPh_3]_4$ were prepared according to previous procedures outlined in the literature (see Supporting Information).[66−72]

Single-Crystal X-ray. Single crystals were covered in Nujol and placed rapidly into the cold N_2 stream of the Kryo-Flex low-temperature device. The data were collected using the SMART[73] software on a Bruker APEX CCD diffractometer using a graphite monochromator with Mo Kα radiation ($\lambda = 0.71073$ Å). For each crystal, a hemisphere of data was collected using a counting time of 30 s per frame. The data were collected at −100 °C. Details of crystal data, data collection, and structure refinement are listed in Table 1. Data reductions were performed using the SAINT[73] software, and the data were corrected for absorption using SADABS.[74] The structures were solved by direct methods using SIR97 and refined by full-matrix least-squares on F^2 with anisotropic displacement parameters for the non-H atoms using SHELXL-97[75] and the WinGX[76] software package. Thermal ellipsoid plots were produced using SHELXTL.[77]

Solid-State NMR. The majority of solid-state NMR experiments were performed at the University of Windsor on a Varian Infinity Plus NMR spectrometer with an Oxford 9.4 T (^1H = 400 MHz) wide-bore magnet operating at $\nu_0(^{65}Cu) = 113.49$ MHz, $\nu_0(^{63}Cu) = 105.85$ MHz, $\nu_0(^{31}P) = 161.81$ MHz, and $\nu_0(^{13}C) = 100.52$ MHz. Experiments were conducted using 5.0 mm HX static, 5.0 mm HXY MAS, and 2.5 mm HX MAS NMR probes. For ^1H-^{13}C cross-polarization magic-angle spinning (CP/MAS) and static $^{63/65}Cu$ NMR experiments, samples were packed into 5.0 mm o.d. zirconia rotors, and for ^1H-^{31}P CP/MAS and $^{63/65}Cu$ MAS NMR experiments, 2.5 mm o.d. zirconia rotors were used. Wide-line copper NMR experiments were performed using a silver coil made from 99.9% silver wire to reduce background signal from copper metal within the probehead. Experiments at 21.1 T (^1H = 900 MHz) were conducted at the National Ultrahigh-field NMR Facility for Solids in Ottawa on a Bruker Avance II spectrometer with a standard-bore magnet. A 5.0 mm single-channel static probe was tuned to ^{65}Cu (ν_0 = 255.74 MHz) or ^{63}Cu (ν_0 = 238.73 MHz) and samples were packed into 5.0 mm o.d. glass tubes.

Air and moisture sensitive samples were packed in a dry nitrogen glovebox and the 5.0 mm zirconia rotors were sealed using airtight Teflon caps. Copper chemical shifts were referenced to $CuCl_{(s)}$ (δ_{iso} = 0.0 ppm), ^{31}P chemical shifts were referenced to phosphoric acid (δ_{iso} = 0.0 ppm) using ammonium dihydrogen phosphate as a secondary standard (δ_{iso} = 0.81 ppm) and ^{13}C resonances were referenced to tetramethylsilane (δ_{iso} = 0.0 ppm) using adamantane as a secondary standard (δ_{iso} = 38.57 ppm for the high-frequency resonance).

Table 1. Summary of X-ray Crystallographic Data for the $Cp'CuPR_3$ Compounds

	$CpCuPEt_3$	$Cp^{\dagger}CuPPh_3$	Cp^*CuPPh_3
empirical formula	$C_{11}H_{20}CuP$	$C_{27}H_{28}CuP$	$C_{28}H_{30}CuP$
fw	246.79	447.01	461.04
T (K)	223	173	173
wavelength (Å)	0.71073	0.71073	0.71073
cryst syst	monoclinic	orthorhombic	monoclinic
space group	$P2_1/m$	$Pna2_1$	$P2_1/c$
unit cell dimensions			
a (Å)	7.5926(7)	15.842(2)	18.795(3)
b (Å)	10.8150(10)	10.1071(14)	15.553(3)
c (Å)	8.5288(8)	14.466(2)	17.690(3)
α (deg)	90	90	90
β (deg)	115.828(2)	90	111.492(2)
γ (deg)	90	90	90
Vol (Å^3)	630.37(10)	2316.3(5)	4811.6(15)
Z	2	4	8
density (calcd) (g cm^{-3})	1.300	1.282	1.273
abs coeff (mm^{-1})	1.818	1.022	0.986
F (000)	260	936	1936
θ range for data collection (deg)	2.65−27.51	2.39−27.50	1.75−27.50
limiting indices	$-9 \le h \le 9$ $-14 \le k \le 14$ $-11 \le l \le 11$	$-20 \le h \le 20$ $-13 \le k \le 13$ $-18 \le l \le 18$	$-23 \le h \le 23$ $-20 \le k \le 20$ $-22 \le l \le 22$
reflns collected	5370	22954	53253
independent reflns	1502	5214	10916
R_{int}	0.034	0.0629	0.0728
absorption correction	SADABS	SADABS	SADABS
refinement method	full matrix least-squares on F^2	full matrix least-squares on F^2	full matrix least-squares on F^2
data/restraints/ parameters	1502/4/70	5214/1/267	10916/0/551
GOF on F^2	1.372	1.206	1.045
final R indices[a] [$I > 2\sigma(I)$]	$R1 = 0.0747$ $wR2 = 0.1646$	$R1 = 0.0696$ $wR2 = 0.1257$	$R1 = 0.0528$ $wR2 = 0.1013$
R indices (all data)	$R1 = 0.0775$ $wR2 = 0.1659$	$R1 = 0.0827$ $wR2 = 0.1333$	$R1 = 0.0945$ $wR2 = 0.1176$
Largest difference map peak and hole (e Å^{-3})	0.668, −0.665	0.725, −0.923	0.614, −0.428

[a] $R1(F) = \{\sum(|F_o| - |F_c|)/\sum|F_o|\}$ for reflections with $F_o > 4(\sigma(F_o))$. $wR2(F^2) = (\sum w(|F_o|^2 - |F_c|^2)^2/\sum w(|F_o|^2)^2\}^{1/2}$ where w is the weight given each reflection.

Frequency-stepped NMR using the Hahn-echo and/or QCPMG pulse sequences were utilized in the static $^{63/65}Cu$ experiments. The Hahn-echo sequence has the form $(\pi/2)_x-\tau_1-(\pi)_y-\tau_2-$acq, where τ represents interpulse delays of 20−30 μs. The QCPMG sequence is similar except that a train of alternating refocusing pulses and acquisition periods follow the initial Hahn-echo sequence.[61] To ensure uniform excitation of the broad powder patterns, the effective excitation bandwidth was determined at a given rf field strength from an individual subspectrum, and then the appropriate transmitter offset size was selected.[63] In wide-line QCPMG experiments, the transmitter frequency is also set as a multiple of the spikelet separation.

Experiments at 9.4 T. $^{63/65}Cu$ MAS NMR experiments were conducted on $[Cu(PhCN)_4]BF_4$ using a Hahn-echo pulse sequence (detailed listings of experimental parameters are given in the Supporting Information). Static Hahn-echo $^{63/65}Cu$ NMR experiments were performed on $[Cu(PhCN)_4]BF_4$, $CpCuPEt_3$, $CpCuPPh_3$, $Cp^{\dagger}CuPPh_3$ and Cp^*CuPPh_3. The $Cp'CuPR_3$ complexes required collection of between 5 and 19 subspectra, using spectral widths of 1000 or 2000 kHz and transmitter frequency offsets of 100 or 200 kHz. For static ^{65}Cu QCPMG NMR experiments, the spectral width for each piece was set between 800 and 2000 kHz. To accommodate the full T_2 decay, the number of Meiboom−Gill (MG) loops were set between 19 and 408 and the acquisition time, τ_a, for each echo was adjusted to attain a spikelet separation ($1/\tau_a$) between 20 and 40 kHz. ^{63}Cu QCPMG NMR experiments were only performed on the $Cp'CuPR_3$ compounds (see

(64) Pangborn, A. B.; Giardello, M. A.; Grubbs, R. H.; Rosen, R. K.; Timmers, F. J. *Organometallics* **1996**, *15*, 1518.
(65) Jardine, F. H.; Rule, L.; Vohra, A. G. *J. Chem. Soc. A* **1970**, 238.
(66) Knaust, J. M.; Knight, D. A.; Keller, S. W. *J. Chem. Cat.* **2003**, *33*, 813.
(67) Cotton, F. A.; Marks, T. J. *J. Am. Chem. Soc.* **1970**, *92*, 5114.
(68) Bowmaker, G. A.; Cotton, J. D.; Healy, P. C.; Kildea, J. D.; Silong, S. B.; Skelton, B. W.; White, A. H. *Inorg. Chem.* **1989**, *28*, 1462.
(69) Badiei, Y. M.; Warren, T. H. *J. Organomet. Chem.* **2005**, *690*, 5989.
(70) Bowmaker, G. A.; Camp, D.; Hart, R. D.; Healy, P. C.; Skelton, B. W.; White, A. H. *Aust. J. Chem.* **1992**, *45*, 1155.
(71) Churchill, M. R.; Kalra, K. L. *Inorg. Chem.* **1974**, *13*, 1427.
(72) Churchill, M. R.; Deboer, B. G.; Donovan, D. J. *Inorg. Chem.* **1975**, *14*, 617.
(73) *SMART Molecular Analysis Research Tool*; Bruker AXS Inc.: Madison, WI, 2001.
(74) *SAINTPlus Data Reduction and Correction Program*; Bruker AXS Inc.: Madison, WI, 2001.
(75) Sheldrick, G. M. *SHELXL-97*; Universitat Gottingen: Gottingen, Germany, 1997.
(76) Farrugia, L. J. *J. Appl. Crystallogr.* **1999**, *32*, 837.
(77) Sheldrick, G. M. *SHELXTL, Structure determination software suite*; Bruker AXS Inc.: Madison, WI, 2001.

Supporting Information for details on all parameters). Proton-decoupled ^{31}P and ^{13}C NMR experiments were performed using the variable-amplitude cross polarization[78,79] (VACP) MAS pulse sequence with a two-pulse phase-modulation (TPPM) decoupling scheme.[80] Full details on ^{31}P and ^{13}C NMR experiments are also given in the Supporting Information.

Experiments at 21.1 T. Static Hahn-echo $^{65/63}$Cu NMR experiments at 21.1 T were conducted only upon $[Cu(PhCN)_4]BF_4$, using a spectral width of 500 kHz, selective $\pi/2$ pulse widths of 1.5−3.0 μs and a recycle delay of 1.0 s, while acquiring 3425 to 4560 scans.

NQR. ^{63}Cu and ^{65}Cu quadrupole frequencies were obtained at ambient temperature, using a Bruker CXP console pulsing into a specially modified NQR probe arrangement that was well removed from the influence of an external magnetic field (>5 m), and shielded from extraneous magnetic and radio frequency interference by a MuMetal container. The quadrupole frequency ranges that were scanned were determined from previous NQR studies of Cu(I) systems.[6,37,81−83] The location of both ^{63}Cu and ^{65}Cu isotope resonances (related by the ratio of the $\nu_Q(^{63}Cu)/\nu_Q(^{65}Cu) = 1.078$) verified that true copper NQR frequencies were being observed. Conventional $\theta-\tau-2\theta-\tau-$acq solid-echo (or Hahn-echo) experiments with extended phase cycles[84] were implemented for the detection of these quadrupole frequencies. A rf power of ~1 kW and short pulses of <1 μs duration were used for excitation of the ($\pm^1/_2$, $\pm^3/_2$) transition. Pulse lengths were optimized with a Cu_2O sample which provides a characteristic quadrupole frequency at 26.01−26.02 MHz at 293 K,[85] with recycle delays typically ranging between 0.1 and 0.5 s.

NMR Simulations. All NMR parameters, including C_Q, η_Q, δ_{iso}, Ω, κ, R_{DD}, and J were determined by analytical simulations of the NMR spectra using the WSolids software package.[86] Numerical simulations of some patterns were conducted using SIMPSON.[87]

Theoretical Calculations. Calculations of $^{63/65}$Cu EFG parameters were performed on dual-733 MHz Pentium III Dell Precision 420, dual-2.8 GHz Xenon Dell Precision 650 or dual-3.6 GHz Xenon Dell Precision 670n workstations. Gaussian 98[88] and Gaussian 03[89] were used for the calculations employing the restricted Hartree−Fock (RHF) method, density functional theory (BLYP),[90,91] and the hybrid density functional theory (B3LYP). The 6-31G**, 6-311G**, 6-31++G**, and 6-311++G** basis sets were used for all atoms, except in some cases where the all-electron basis set of Huzinaga (14s8p5d) was used for the copper atoms.[92] The Amsterdam density functional (ADF) suite[93−95] was used to calculate EFG parameters for a select number of compounds. The BLYP[90,91] and VWN+BP[96−98] exchange-and-correlation functionals were applied, and DZ and TZP basis sets provided with the ADF package were used on all atoms.

Results and Discussion

This section of the paper is outlined as follows: First, we discuss the acquisition and interpretation of ^{65}Cu and ^{63}Cu solid-state NMR spectra for the series of complexes outlined above (Chart 1). Frequency-stepped wide-line and/or wide-line QCPMG NMR spectra are shown for all samples but $[Cu(PhCN)_4]BF_4$, for which standard MAS and Hahn-echo NMR spectra were acquired. Spectral simulations and corresponding NMR parameters are given for each sample, and copper CS tensor data are also presented where appropriate. ^{31}P CP/MAS NMR spectra are then presented for all complexes with Cu−P spin pairs, and comments are made on the molecular EFG tensor orientations, the signs of C_Q, and anisotropic J-coupling parameters. Finally, first principles calculations of copper EFG and CS tensors are presented, along with discussion on the suitability of basis sets and methods, as well as the relationships between tensor parameters and molecular structure.

Solid-State ^{63}Cu and ^{65}Cu NMR. $[Cu(PhCN)_4]BF_4$. $[Cu(PhCN)_4]BF_4$ is distinct from the other complexes discussed herein, since the Cu atom exists in a relatively spherically symmetric environment. We present spectra of this complex as a "low-limit" comparison to our other samples, since the quadrupolar interaction arising from this environment is small enough to permit routine NMR experiments as well as demonstrating the influence of copper CSA on ^{65}Cu and ^{63}Cu NMR spectra. Analytical simulations of ^{65}Cu and ^{63}Cu MAS NMR spectra (Figure 1a) yield C_Q values comparable to those reported by Wasylishen et al. for $K_3Cu(CN)_4$ ($C_Q(^{63}Cu) = -1.125$ MHz and $C_Q(^{65}Cu) = -1.040$ MHz).[10] We note here that the signs of C_Q reported by Wasylishen et al. are determined via residual dipolar couplings observed in ^{13}C NMR spectra. Signs of C_Q are not directly obtainable from $^{63/65}$Cu NMR spectra, and we report the absolute values of C_Q (i.e., $|C_Q(^{63}Cu)|$ and $|C_Q(^{65}Cu)|$). The issue of signs will be addressed below in the ^{31}P NMR section. Interestingly, η_Q are distinct in these pseudotetrahedral systems, with values of 0.95(5) and 0.0 for $[Cu(PhCN)_4]BF_4$ and $K_3Cu(CN)_4$, respectively. The larger C_Q and nonzero η_Q in $[Cu(PhCN)_4]BF_4$ arise from the relatively distorted tetrahedral geometry about the copper atom in comparison to $K_3Cu(CN)_4$ (Table S5).

Static Hahn-echo NMR spectra of $[Cu(PhCN)_4]BF_4$ were acquired in single experiments at 9.4 and 21.1 T (Figure 1b,c). Comparison of these spectra and simulation of the powder patterns using only quadrupolar parameters reveal a strong anisotropic copper shielding contribution with a span of 260(10) ppm (Table 2). The Euler angles indicate that the largest component of the EFG tensor and most shielded component of the CS tensor are not co-incident. To the best of our knowledge, there are few reports of copper CSA, including $\Omega = 42$ ppm for $K_3Cu(CN)_4$[10] and $\Omega = 350-750$ ppm for polycrystalline copper dialkyldithiophosphate clusters.[15−18] The span observed for $[Cu(PhCN)_4]BF_4$ is much larger than $K_3Cu(CN)_4$, again undoubtedly due to its distorted tetrahedral environment.

(78) Peersen, O. B.; Wu, X. L.; Kustanovich, I.; Smith, S. O. *J. Magn. Reson., Ser. A* **1993**, *104*, 334.
(79) Peersen, O. B.; Wu, X. L.; Smith, S. O. *J. Magn. Reson., Ser. A* **1994**, *106*, 127.
(80) Bennett, A. E.; Rienstra, C. M.; Auger, M.; Lakshmi, K. V.; Griffin, R. G. *J. Chem. Phys.* **1995**, *103*, 6951.
(81) Bowmaker, G. A. *Adv. Spectrosc.* **1987**, *14*, 1.
(82) Kroeker, S.; Hanna, J. V.; Wasylishen, R. E.; Ainscough, E. W.; Brodie, A. M. *J. Magn. Res.* **1998**, *135*, 208.
(83) Ainscough, E. W.; Brodie, A. M.; Burrell, A. K.; Freeman, G. H.; Jameson, G. B.; Bowmaker, G. A.; Hanna, J. V.; Healy, P. C. *J. Chem. Soc., Dalton Trans.* **2001**, 144.
(84) Kunwar, A. C.; Turner, G. L.; Oldfield, E. *J. Magn. Res.* **1986**, *69*, 124.
(85) Biryukov, I. P.; Voronkov, M. G.; Safin, I. A. *Tables of Nuclear Quadrupole Resonance Frequencies;* Israel Program for Scientific Translations: Jerusalem, Israel, 1969.
(86) Eichele, K.; Wasylishen, R. E. *WSolids1: Solid-State NMR Spectrum Simulation*, version 1.17.30; University of Tübingen, Tübingen, Germany, 2001.
(87) Bak, M.; Rasmussen, J. T.; Nielsen, N. C. *J. Magn. Res.* **2000**, *147*, 296.
(88) Frisch, M. J.; et al. *Gaussian 98*; revision A.9; Gaussian, Inc.: Pittsburgh, PA, 1998.
(89) Frisch, M. J.; et al. *Gaussian 03*; revision B.03; Gaussian, Inc.: Pittsburgh, PA, 2003.
(90) Becke, A. D. *Phys. Rev. A* **1988**, *38*, 3098.
(91) Lee, C.; Yang, W.; Parr, R. G. *Phys. Rev. B* **1988**, *37*, 785.
(92) Huzinaga, S.; Andzelm, J. *Gaussian Basis Sets for Molecular Calculations*; Elsevier: New York, 1984; Vol. 16.
(93) *ADF2005.01*; SCM, Theoretical Chemistry, Vrije Universiteit: Amsterdam, The Netherlands, 2005.
(94) Velde, G. T.; Bickelhaupt, F. M.; Baerends, E. J.; Guerra, C. F.; Van Gisbergen, S. J. A.; Snijders, J. G.; Ziegler, T. *J. Comput. Chem.* **2001**, *22*, 931.
(95) Guerra, C. F.; Snijders, J. G.; te Velde, G.; Baerends, E. J. *Theor. Chem. Acc.* **1998**, *99*, 391.
(96) Vosko, S. H.; Wilk, L.; Nusair, M. *Can. J. Phys.* **1980**, *58*, 1200.
(97) Perdew, J. P. *Phys. Rev. B* **1986**, *34*, 7406.
(98) Perdew, J. P. *Phys. Rev. B* **1986**, *33*, 8822.

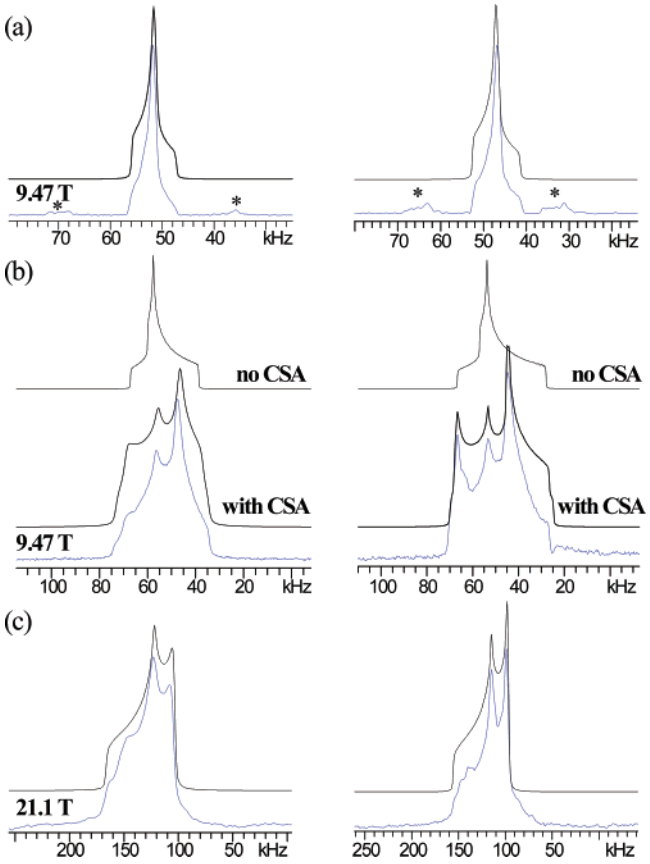

Figure 1. ^{65}Cu (left set) and ^{63}Cu (right set) NMR spectra of $[Cu(PhCN)_4]BF_4$: (a) simulation and experimental MAS spectra at 9.4 T with ν_{rot} = 16.0 kHz; (b) static NMR spectra at 9.4 T; and (c) static NMR spectra at 21.1 T. The asterisks (∗) indicates spinning sidebands.

Cp′CuPR$_3$ Complexes. ^{63}Cu and ^{65}Cu wide-line QCPMG NMR are shown for the Cp′CuPR$_3$ compounds (Cp′ = Cp, Cp†, Cp*; R = Et, Ph) in Figure 2. As is obvious from the breadths of these powder patterns (700−1300 kHz), the quadrupolar interaction is much larger than that of the four-coordinate species discussed above, owing to the reduction of spherical symmetry about the copper site.[99] The QCPMG pulse sequence is of some benefit here, since it improves the signal-to-noise ratio (*S*/*N*) and reduces the experiment times; however, the increase in the integrated intensity of the spectra is highly dependent upon the copper transverse relaxation (T_2) values (Figures S6 and S7).

Analytical simulations of the QCPMG spectra yield the quadrupolar parameters (Table 2). In all cases, η_Q is close to zero, indicating that the EFG tensors are essentially axially symmetric (i.e., $|V_{11}| \cong |V_{22}| < |V_{33}|$). The orientations of the EFG tensors are constrained by symmetry elements of the molecule; in these systems, the largest components of the EFG tensor, V_{33}, should be oriented along or near the pseudo-3-fold rotational axis of the molecule. It follows that the similarity of V_{11} and V_{22} arises from these components being oriented in very similar environments, perpendicular to this axis. The quadrupolar parameters can be interpreted in terms of the molecular geometries and substituents of these molecules. Structural data is taken from a previously reported single-crystal X-ray experiment on CpCuPPh$_3$,[100] and crystal structures for CpCuPEt$_3$, Cp†CuPPh$_3$, and Cp*CuPPh$_3$ are reported in this work (we reacquired the single-crystal X-ray structure of CpCuPEt$_3$ to obtain the ethyl positions, which were not previously reported).[101] The arrangement of the Cp$_{cent}$, Cu, and P positions (where Cp$_{cent}$ denotes the geometric center of the Cp′ ring) is nearly linear in all of these molecules, with Cp$_{cent}$−Cu−P angles ranging from ca. 170° to 178° (Table S5). The η_Q is a good indicator of linearity, varying from 0.01 for CpCuPEt$_3$ to 0.07 for Cp†CuPPh$_3$, which have Cp$_{cent}$−Cu−P angles closest to and furthest from 180°, respectively. Variations in C_Q can be rationalized by considering the nature of the substituents and their coordination to the copper atom. For the PPh$_3$ complexes, the C_Q increases in a linear fashion with increasing Cp$_{cent}$−Cu distance. The Cp$_{cent}$−Cu distance decreases with increasing ring substitution (Table S5), which is a well-known behavior for many transition-metal metallocenes.[102−106] The Cu−P distances also decrease with increasing ring substitution, though the correlation with C_Q is not linear. The C_Q is the largest in the CpCuPEt$_3$ complex, which has very similar Cp$_{cent}$−Cu and Cu−P bond lengths to those of CpCuPPh$_3$; hence, it is not strictly the atomic positions which determine the magnitude of the EFG tensor components, but also the electronic properties of the substituents. This is addressed further in the theoretical section below.

Copper CSA also makes a significant contribution to the appearance of the powder patterns. The spans range from ca. 1200 to 1500 ppm (the largest reported to date), and are comparable to the copper chemical shift range for molecular copper species (ca. 1000 ppm).[107,108] Values of κ are between 0.90 and 0.95, indicating that the CS tensor is almost axially symmetric and that the most shielded component of the tensors, δ_{33}, is the unique component. The Euler angle β is close to zero, indicating that the V_{33} and δ_{33} components are nearly coincident with each other, concomitant with the symmetry of the molecule.

ClCuP(2,4,6)$_3$. The static ^{65}Cu QCPMG NMR spectrum of ClCuP(2,4,6)$_3$ is shown in Figure 3a. The breadth of the central transition powder pattern is ca. 5.12 MHz, requiring the collection of 31 subspectra with a total experimental time of 15.5 h. Analytical simulations of this spectrum indicate that C_Q (^{65}Cu) is 60.6(3) MHz and η_Q = 0.25(1). Large C_Q values like this (i.e., 30 to 94 MHz) are normally obtained from NQR experiments.[37,82] To the best of our knowledge, the largest C_Q previously measured by solid-state NMR was reported for polycrystalline $[Cu_6\{S_2P(OiBu)_2\}_6]$, having a C_Q(^{65}Cu) value of 47.6(2) MHz and a η_Q of 0.10.[16] The magnitude of C_Q in ClCuP(2,4,6)$_3$ is much larger than those of the metallocenes, largely because of the two-coordinate, nearly linear (∠Cl−Cu−P

(99) Kentgens, A. P. M. *Geoderma* **1997**, *80*, 271.
(100) Cotton, F. A.; Takats, J. *J. Am. Chem. Soc.* **1970**, *92*, 2353.
(101) Delbaere, L. T.; McBride, D. W.; Ferguson, R. B. *Acta Crystallogr., Sect. B* **1970**, *B26*, 515.
(102) Fitzpatrick, P. J.; Lepage, Y.; Sedman, J.; Butler, I. S. *Inorg. Chem.* **1981**, *20*, 2852.
(103) Fortier, S.; Baird, M. C.; Preston, K. F.; Morton, J. R.; Ziegler, T.; Jaeger, T. J.; Watkins, W. C.; Macneil, J. H.; Watson, K. A.; Hensel, K.; Lepage, Y.; Charland, J. P.; Williams, A. J. *J. Am. Chem. Soc.* **1991**, *113*, 542.
(104) Martin, A.; Mena, M.; Palacios, F. *J. Organomet. Chem.* **1994**, *480*, C10.
(105) Engelhardt, L. M.; Papasergio, R. I.; Raston, C. L.; White, A. H. *Organometallics* **1984**, *3*, 18.
(106) Pevec, A. *Acta Cim. Slov.* **2003**, *50*, 199.
(107) Goodfellow, R. J. Post-Transition Metals, Copper to Mercury. In *Multinuclear NMR*; 1st ed.; Mason, J., Ed.; Plenum Press: New York, 1987; pp 521.
(108) Malito, J. Copper-63 NMR Spectroscopy. In *Annual Reports on NMR Spectroscopy*; Webb, G. A., Ed.; Academic Press: London, 1999; Vol. 38, pp 265.

Table 2. Experimental $^{65/63}$Cu NMR Parameters

compound		δ_{iso} (ppm)[a]	$\lvert C_Q(^{65}Cu)\rvert$ (MHz)[b]	$\lvert C_Q(^{63}Cu)\rvert$ (MHz)[b]	η_Q [c]	Ω (ppm)[d]	κ[e]	α (deg)	β (deg)	γ (deg)
$[Cu(PhCN)_4]BF_4$		−510(5)	3.63(10)	4.10(10)	0.95(5)	260(10)	−0.38(4)	92(2)	92(2)	24(3)
$CpCuPEt_3$		150(50)	32.2(2)	34.7(3)	0.01(1)	1500(200)	0.90(10)	0	0	0
$CpCuPPh_3$		−50(50)	29.4(2)	31.7(3)	0.03(1)	1500(300)	0.95(5)	0	0	0
$Cp^{\dagger}CuPPh_3$		0(80)	25.4(3)	27.4(4)	0.07(2)	1300(200)	0.95(5)	0	0	0
Cp^*CuPPh_3		−50(50)	24.3(2)	26.2(3)	0.05(3)	1200(200)	0.95(5)	0	0	0
$ClCuP(2,4,6)_3$		170(50)	60.6(3)	65.3[f]	0.25(1)					
$(hfac)CuPMe_3$		125(100)	52.5(5)	56.6[f]	0.85(5)					
$[Me_3NN]Cu(CNAr)$		1050(200)	71.0(1)	76.6[f]	0.11(1)					
$[ClCuPPh_2Mes]_2$		100(200)	51.2(6)	55.2[f]	0.50(2)	1100(400)	−0.70(20)	10(10)	90(15)	30(10)
$[BrCuPPh_2Mes]_2$		200(250)	50.2(3)	54.1[f]	0.55(2)	1000(700)	−0.90(10)	20(10)	90(15)	10(10)
$[ICuPPh_2Mes]_2$		100(100)	46.9(2)	50.6[f]	0.48(2)	1100(500)	−0.90(10)	10(10)	90(10)	10(10)
$[BrCuPPh_3]_4 \cdot 2CHCl_3$	trigonal	−100(100)	51.0(3)	55.0[f]	0.39(2)					
	tetrahedral	210(25)	23.5(4)	25.3[f]	0.79(3)					
$[ICuPPh_3]_4$	trigonal	−50(50)	47.5(4)	51.2[f]	0.49(2)					
	tetrahedral	290(25)	22.0(4)	23.7[f]	0.36(2)	300(100)[g]	0.20(10)	0	0	0

[a] Isotropic chemical shift: $\delta_{iso} = (\delta_{11} + \delta_{22} + \delta_{33})/3$. [b] Quadrupole coupling constant: $C_Q = e^2qQV_{33}/h$. [c] Asymmetry parameter: $\eta_Q = (V_{11} - V_{22})/V_{33}$. [d] Span: $\Omega = \delta_{11} - \delta_{33}$. [e] Skew: $\kappa = 3(\delta_{22} - \delta_{iso})/\Omega$. [f] Calculated C_Q values using the ratio of the ^{63}Cu and ^{65}Cu quadrupole moments: $Q(^{63}Cu)/Q(^{65}Cu) = 1.0784$. [g] See Figure S12 and associated text in the Supporting Information.

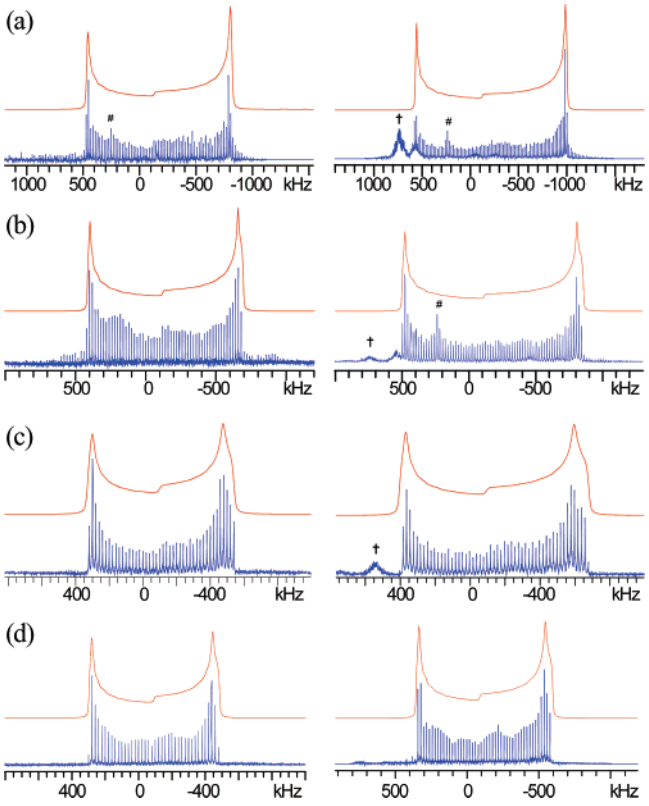

Figure 2. Static ^{65}Cu (left) and ^{63}Cu (right) NMR spectra of (a) $CpCuPEt_3$, (b) $CpCuPPh_3$, (c) $Cp^{\dagger}CuPPh_3$, and (d) Cp^*CuPPh_3. Top and bottom traces are analytical simulations and experimental spectra, respectively. The dagger (†) denotes FM radio signal interference and the pound (#) indicates NMR signal from copper metal from the probe.

= 172.68°), spherically asymmetric environment of the Cu atom. As in the case of the metallocenes, V_{33} is the distinct component of the EFG tensor, and is likely oriented along or near the Cu−P bond, which is contained within a pseudo-3-fold axis of the molecule. The slightly nonlinear arrangement of atoms orients V_{11} and V_{22} in two slightly differing electronic environments, giving rise to the nonaxially symmetric η_Q. Even a large copper CSA will only make a minor contribution to the overall pattern (Figure S8), so no comment can be made on the nature of the anisotropic CS tensor in this case.

Trigonal Planar Copper Compounds. Static ^{65}Cu NMR spectra of $(hfac)CuPMe_3$ and $[Me_3NN]Cu(CNAr)$ are shown in Figure 3b,c. Simulations of these powder patterns yield C_Q values of 52.5(5) and 71.0(1) MHz for $(hfac)CuPMe_3$ and $[Me_3NN]Cu(CNAr)$, respectively. These C_Q values, in addition to that of $ClCuP(2,4,6)_3$, are among the largest C_Q values measured to date by solid-state NMR. An interesting difference in spectral features of these copper complexes are the values of η_Q, which are 0.85(5) and 0.11(1) for $(hfac)CuPMe_3$ and $[Me_3NN]Cu(CNAr)$, respectively. In both of these trigonal planar complexes, it is expected that V_{33} is oriented perpendicular to the trigonal plane, in accordance with previous experimental and theoretical studies on quadrupolar nuclei in planar three-coordinate environments.[63,109] In addition, it would be expected that V_{22} would be oriented along or near the Cu−P or Cu−C bonds in $(hfac)CuPMe_3$ and $[Me_3NN]Cu(CNAr)$, respectively. However, in the former case, V_{22} is almost of the same magnitude as V_{33}, with V_{11} being the distinct component, which is unusual for such coordination environments (see the theoretical section below).

$[XCuPPh_2Mes]_2$ (X = Cl, Br, I). Static ^{65}Cu QCPMG NMR spectra of $[XCuPPh_2Mes]_2$ are shown in Figure 4. The C_Q values for these systems (Table 2) are consistent with those determined by NQR data (Table 3). Simulations using full diagonalizations of the combined Zeeman and quadrupolar Hamiltonians do not affect the shape or breadth of the powder patterns in comparison to analytical or numerical simulations using first-order perturbation theory (Figure S9).[110] This indicates that the high-field approximation is still valid under these conditions. In contrast to the metallocene complexes, the values of C_Q are observed to increase with decreasing first-coordination sphere bond lengths and increasing formal negative charge on the X atom in the $[XCuPPh_2Mes]_2$ series (Table S5). A similar trend has also been observed for other trigonal planar complexes.[63] Similar to $(hfac)CuPMe_3$ and $[Me_3NN]Cu(CNAr)$, the V_{33} component of the $^{63/65}$Cu EFG tensor is expected to be oriented perpendicular to the trigonal plane. Since η_Q is close to 0.5, V_{11} and V_{22} are distinct from one another, with one of these components likely oriented near or along the Cu−P bond. These spectra are also

(109) Hansen, M. R.; Madsen, G. K. H.; Jakobsen, H. J.; Skibsted, J. *J. Phys. Chem. A* **2005**, *109*, 1989.
(110) Bain, A. D. *Mol. Phys.* **2003**, *101*, 3163.

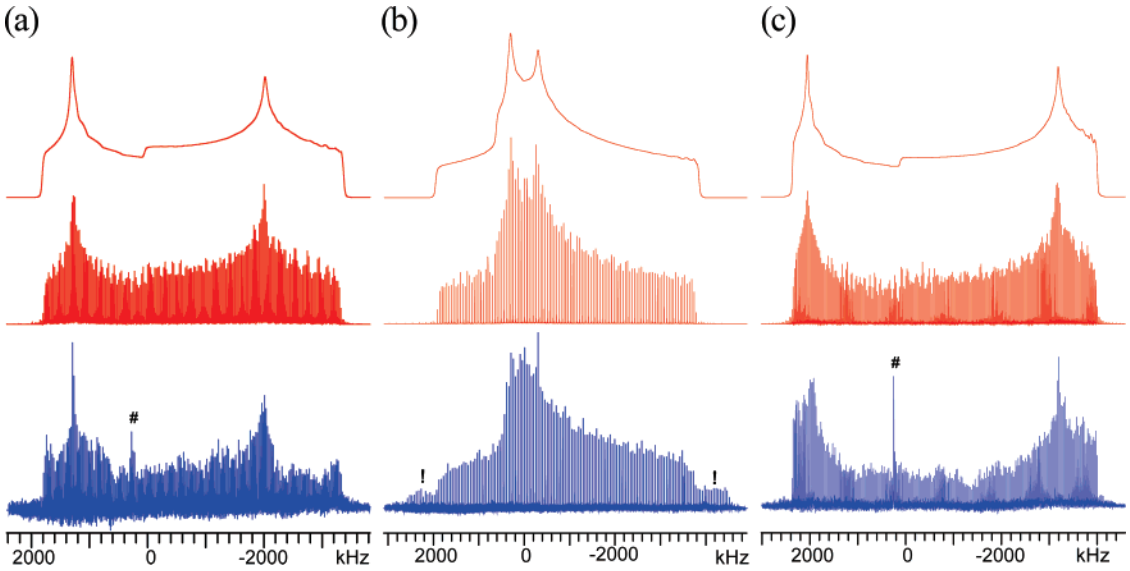

Figure 3. Static ^{65}Cu NMR spectra of (a) ClCuP(2,4,6)$_3$, (b) (hfac)CuPMe$_3$, and (c) [Me$_3$NN]Cu(CNAr). Top, middle, and bottom traces are analytical simulations, numerical simulations, and experimental spectra, respectively. The pound sign (#) denotes copper metal interference and exclamation point (!) indicates part of the satellite transitions.

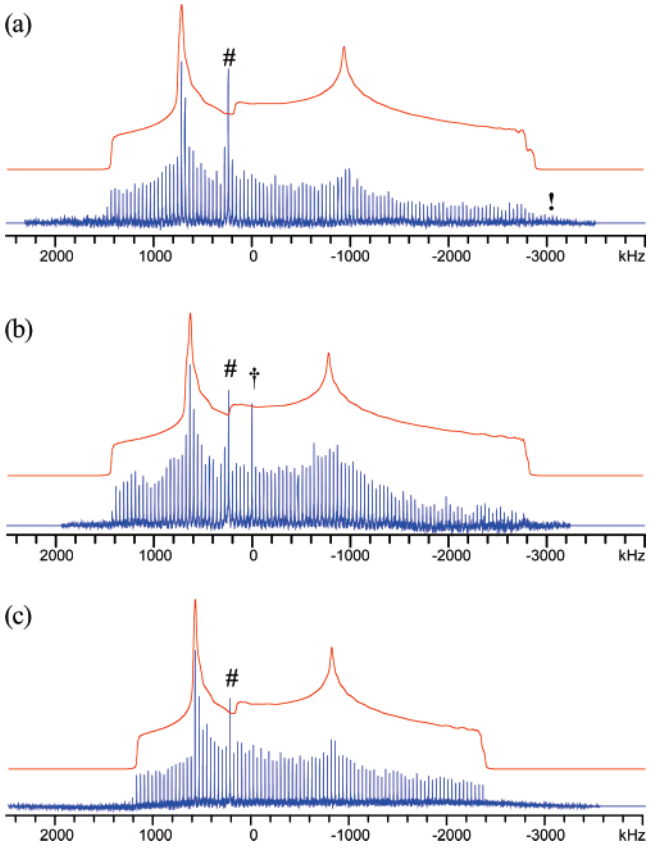

Figure 4. Static ^{65}Cu QCPMG spectra of (a) [ClCuPPh$_2$Mes]$_2$, (b) [BrCuPPh$_2$Mes]$_2$, and (c) [ICuPPh$_2$Mes]$_2$. Top and bottom traces are analytical simulations and experimental spectra respectively. The pound sign (#) denotes copper metal interference, the dagger (†) indicates a processing artifact, and the exclamation point (!) indicates the signal from $\pm$ $^1/_2$ $\leftrightarrow$ $^3/_2$ satellite transitions.

influenced by copper CSA (Figure S10), with Ω values ca. 1000−1100 ppm. In contrast to the metallocene complexes, the negative skews designate δ_{11} as the distinct CS tensor component, which is consistent with the relative orientation of the EFG and CS tensors predicted by the Euler angles for each complex, which have V_{33} and δ_{11} oriented closely together (i.e., δ_{11} is perpendicular to the trigonal plane).

[BrCuPPh$_3$]$_4$·2CHCl$_3$ and [ICuPPh$_3$]$_4$. For very broad central transition powder patterns it is not possible to distinguish multiple sites using techniques such as MQMAS, because of the current limitations on spinning speeds and bandwidth excitations. Frequency-stepped wide-line NMR can be used to resolve multiple sites only if they have fairly distinct quadrupolar parameters. The ^{65}Cu NMR spectra of the [BrCuPPh$_3$]$_4$·2CHCl$_3$ and [ICuPPh$_3$]$_4$ "stepped" clusters reveal two overlapping patterns (Figure 5), with the narrower central patterns corresponding to the smaller values of C_Q in each case. The broad underlying patterns do not arise from the $\pm$ $^1/_2$ $\leftrightarrow$ $^3/_2$ satellite transitions, since analytical simulations of, for example, [ICuPPh$_3$]$_4$ indicate that the most intense portions of the satellite transitions would be approximately $\pm$3.5 MHz from the central transition (Figure S11). Since the sharp discontinuities of the underlying pattern occur at ca. $\pm$700 kHz, this is clearly a central transition pattern from a second Cu site with larger values of C_Q (Table 2).

Single-crystal X-ray diffraction data indicates that there are three- and four-coordinate sites in these cluster compounds.[71,72] The three-coordinate sites are trigonal planar (CuX$_2$PPh$_3$), whereas the four coordinate sites are distorted tetrahedra (CuX$_3$PPh$_3$) (see Table S5 for structural details). Since the latter have higher spherical symmetry, the patterns with smaller C_Q values are assigned to the four-coordinate sites, and those with the large C_Q values to the three-coordinate sites. Similar values have been previously reported in NQR studies.[34,111,112] For the three-coordinate environment, V_{33} should be oriented perpendicular to the molecular trigonal plane. Although the X−Cu bond lengths are approximately the same for the respective compounds, ca. 2.40 and 2.56 Å for X = Br and I, respectively, the two X−Cu−P bond angles differ significantly, with ($\angle$Br−Cu−P) = 118.97° and 128.75° and ($\angle$I−Cu−P) = 114.18° and 127.49°. Hence, V_{11} and V_{22} are oriented in different environments, accounting for the nonzero values of η_Q. For the

(111) Eller, P. G.; Kubas, G. J.; Ryan, R. R. *Inorg. Chem.* **1977**, *16*, 2454.
(112) Negita, H.; Hiura, M.; Yamada, K.; Okuda, T. *J. Mol. Struct.* **1980**, *58*, 205.

Table 3. NQR Data for Select Copper Phosphines

compound	ν_Q (^{63}Cu) (MHz)	C_Q(^{63}Cu)[a] (MHz)	ν_Q (^{65}Cu) (MHz)	C_Q(^{65}Cu)[a] (MHz)	ref
$[ClCu(PPh_3Mes)]_2$	29.35(1)	56.40	27.23(1)	52.32	this work
$[BrCu(PPh_3Mes)]_2$	28.22(1)	53.79	26.18(1)	49.90	this work
$[ICu(PPh_3Mes)]_2$	26.63(1)	51.32	24.70(1)	47.61	this work
$[BrCuPPh_3]_4$·$2CHCl_3$-step; trigonal site	28.09	54.81			34
$[ICuPPh_3]_4$·$2CHCl_3$-step; trigonal site	26.09	50.21			34

[a] Calculation of C_Q was performed using the equation $\nu_Q = C_Q(1 + \eta^2/3)^{1/2}/(S+1/2)$ using η_Q determined from the NMR spectra.[123]

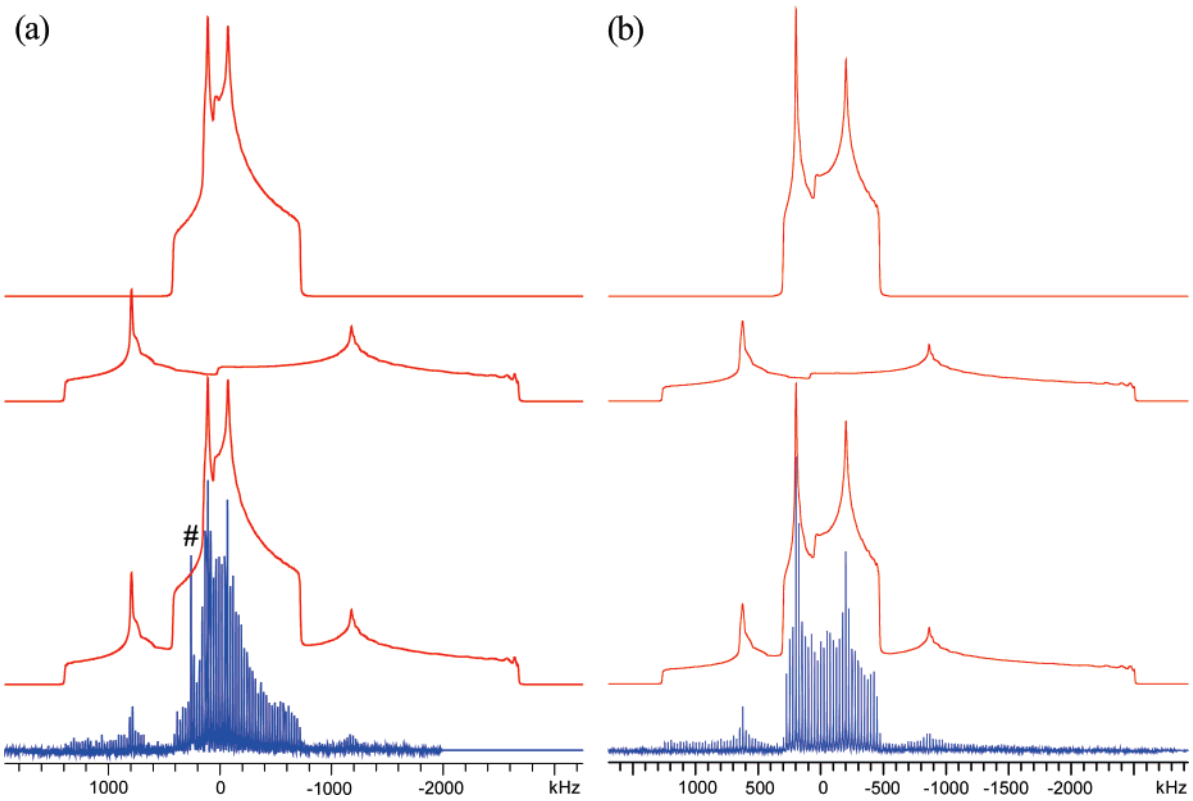

Figure 5. Static ^{65}Cu NMR spectra of (a) $[BrCuPPh_3]_4$·$2CHCl_3$ and (b) $[ICuPPh_3]_4$ stepped clusters. Starting from the top, traces correspond to analytical simulations of the tetrahedral and trigonal sites, the added analytical simulations, and the experimental spectrum.

four-coordinate environment, V_{33} is distinct and oriented along or near the Cu−P bond axis.

Copper Chemical Shifts. The chemical shifts reported for most of the complexes within this paper exist within the standard copper chemical-shift range;[107] however, chemical shifts for copper environments in metallocenes and trigonal planar and linear environments have not previously been observed or reported.[108] A pictorial summary of copper chemical shifts reported herein is shown in Figure 6. It is important to note that the errors associated with many of these chemical shifts are quite large, because of the large breadths of the central transition patterns. The metallocene complexes have copper chemical shifts ranging from ca. 0 to −150 ppm with respect to $CuCl_{(s)}$. Though no previous copper NMR data exists for metallocene complexes, these shifts occur near or at low frequency of the standard, which is commonly observed for most other main group and transition metal metallocenes.[113−116] The molecules with trigonal planar bonding arrangements, $[Me_3NN]$-Cu(CNAr), (hfac)$CuPMe_3$, $[XCuPPh_2Mes]_2$, $[BrCuPPh_3]_4$-·$2CHCl_3$, and $[ICuPPh_3]_4$ have chemical shifts ranging from +1050 to −50 ppm. The copper nucleus in $ClCuP(2,4,6)_3$ is deshielded with respect to the metallocene complexes, and the tetrahedral copper nuclei of $[BrCuPPh_3]_4$·$2CHCl_3$, $[ICuPPh_3]_4$, and $[Cu(PhCN)_4]BF_4$ are even further deshielded. Clearly, there are no simple correlations between the isotropic chemical shifts and the coordination geometry or the chemical nature (e.g., electronegativities) of the first coordination sphere atoms. We can only note that complexes with Cu−P bonds seem to have lower frequency chemical shifts (copper nuclei are more shielded) in comparison to complexes lacking such bonds. The disparity in isotropic chemical shifts is quite dramatic, and a thorough examination of the origin of the chemical shifts of these species is beyond the scope of this paper. As a final note, within some of the NMR spectra, there are cases where resonances from small amounts of copper metal (background from the probe) are observed ($\delta_{iso} \approx 2300$ ppm).[107,117]

(113) Buhl, M.; Hopp, G.; von Philipsborn, W.; Beck, S.; Prosenc, M. H.; Rief, U.; Brintzinger, H. H. *Organometallics* **1996**, *15*, 778.
(114) Schurko, R. W.; Hung, I.; Macdonald, C. L. B.; Cowley, A. H. *J. Am. Chem. Soc.* **2002**, *124*, 13204.
(115) Schurko, R. W.; Hung, I.; Schauff, S.; Macdonald, C. L. B.; Cowley, A. H. *J. Phys. Chem. A* **2002**, *106*, 10096.
(116) Lo, A. Y. H.; Bitterwolf, T. E.; Macdonald, C. L. B.; Schurko, R. W. *J. Phys. Chem. A* **2005**, *109*, 7073.
(117) Lutz, O.; Oehler, H.; Kroneck, P. *Z. Naturforsch., A: Phys. Sci.* **1978**, *33*, 1021.

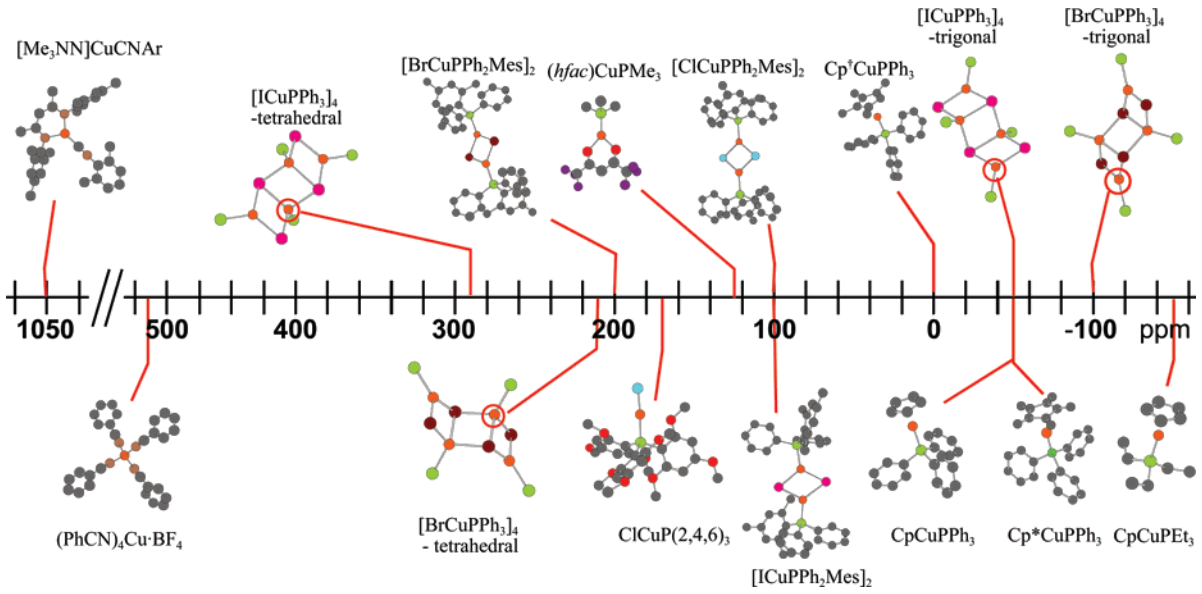

Figure 6. Copper chemical shifts of Cu(I) complexes referenced with respect to $CuCl_{(s)}$ ($\delta_{iso} = 0$ ppm).

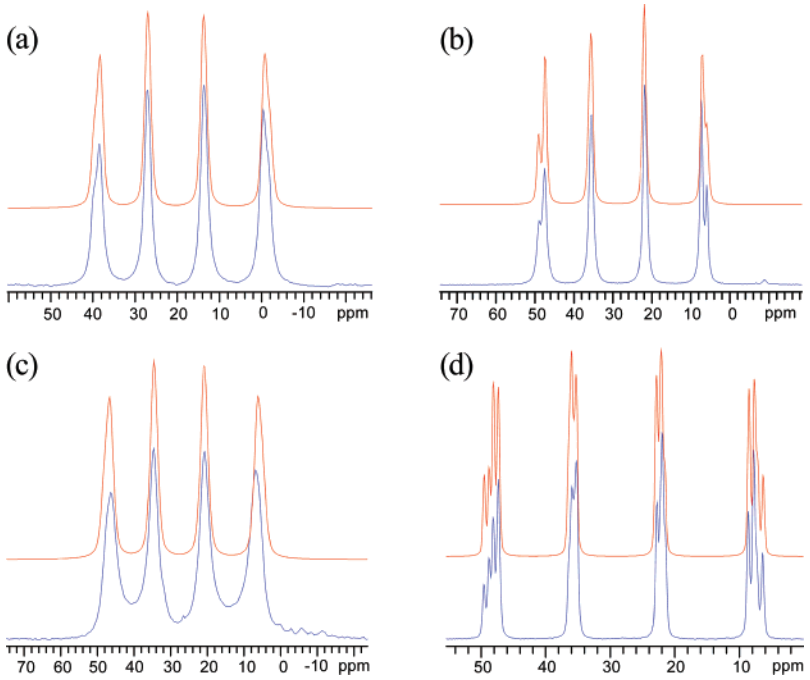

Figure 7. ^{1}H-^{31}P CP/MAS NMR spectra of (a) $CpCuPEt_3$, (b) $CpCuPPh_3$, (c) $Cp^{\dagger}CuPPh_3$, and (d) $Cp^{*}CuPPh_3$. Top and bottom traces are analytical simulations and experimental spectra.

^{31}P CP/MAS NMR and Residual Dipolar Couplings. Although the magnitude of C_Q provides information on the degree of spherical symmetry of the electron distribution about a nucleus, the sign of C_Q gives information on whether V_{33} is increasing or decreasing as one moves outward from the nucleus of interest, and whether a component is pointing into a region of high or low electron density.[109,118] Mössbauer spectroscopy is commonly used to directly obtain the sign of C_Q; however, this is limited to a select number of nuclei with low-energy first excited states.[119] Direct determination of the sign of C_Q by NQR or NMR is not possible since the ordering of energy levels (e.g., $+^1/_2 \rightarrow -^1/_2$ or $-^1/_2 \rightarrow +^1/_2$) have no effect on the magnitude of the quadrupolar frequencies or spectral appearance. However, when quadrupolar nuclei are spin−spin coupled to spin-$^1/_2$ nuclei and residual dipolar couplings are observed in the spin-$^1/_2$ NMR spectrum, it is possible in certain instances to obtain information on both the sign of C_Q and the orientation of the V_{33} component of the EFG tensor with respect to the dipolar vector.[48,49]

The ^{31}P CP/MAS NMR spectra and their corresponding simulations are shown in Figures 7−9, with experimental parameters listed in Table 4. The positions of phosphorus peaks,

(118) Jager, B.; Paluch, S.; Zogal, O. J.; Wolf, W.; Herzig, P.; Filippov, V. B.; Shitsevalova, N.; Paderno, Y. *J. Phys.: Condens. Matter* **2006**, *18*, 2525.
(119) Lucken, E. A. C. *Nuclear Quadrupole Coupling Constants*; Academic Press: London, 1969.

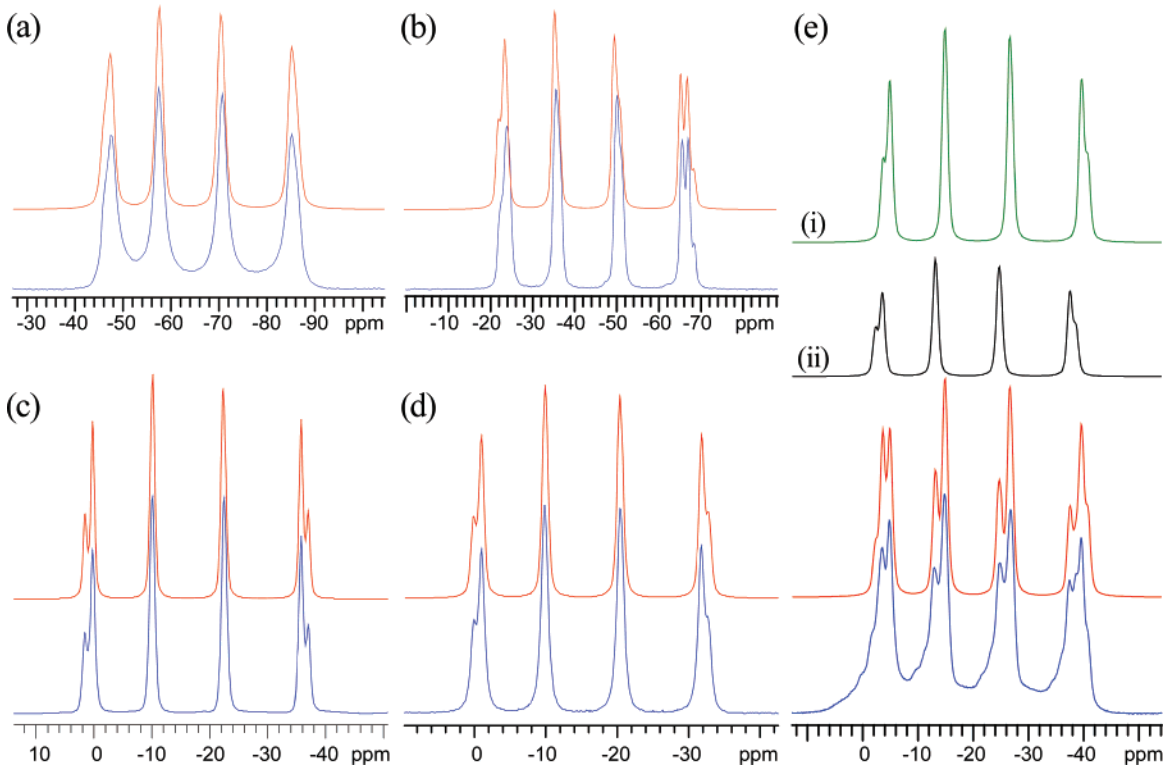

Figure 8. ^{1}H-^{31}P CP/MAS NMR of (a) $ClCuP(2,4,6)_3$, (b) $(hfac)CuPMe_3$, (c) $[ClCuPPh_2Mes]_2$, (d) $[ICuPPh_2Mes]_2$, and (e) $[BrCuPPh_2Mes]_2$. Bottom traces are experimental spectra and top traces are analytical simulations where the two sites, i and ii, are in a 5:3 ratio for trace e.

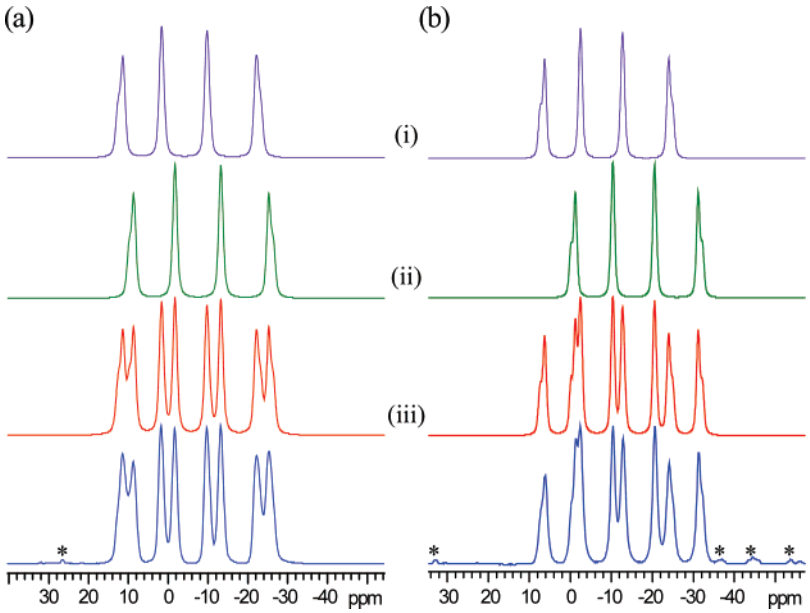

Figure 9. ^{1}H-^{31}P CPMAS NMR spectra of step clusters (a) $[BrCuPPh_3]_4 \cdot 2CHCl_3$ and (b) $[ICuPPh_3]_4$. Top traces are simulations and bottom traces are experimental spectra: (i) simulation of the trigonal site, (ii) simulation of the tetrahedral site, and (iii) the sum of both simulations. The asterisks (∗) denote spinning sidebands.

ν_m, with respect to the frequency of the isotropic chemical shift, ν_{iso}, are determined by

$$\nu_m = \nu_{iso} - mJ_{iso} + \frac{I(I+1) - 3m^2}{I(2I-1)} d$$

where I is the nuclear spin of the quadrupolar nucleus, $m = I$, $I - 1$,..., $-I$, J_{iso} is the isotropic indirect spin−spin coupling and d is the residual dipolar coupling, which is defined as

$$d = \left(\frac{3C_Q R_{eff}}{20\nu_I}\right)[(3\cos^2\beta^D - 1) + \eta_Q \sin^2\beta^D \cos 2\alpha^D]$$

Here, R_{eff} is the effective dipolar coupling constant, defined as $R_{eff} = R_{DD} - \Delta J/3$, ν_I is the Larmor frequency of the quadrupolar nucleus, and α^D and β^D are angles defining the

Table 4. ^{31}P NMR Experimental Parameters.

compound		δ_{iso} (ppm)	C_Q (MHz)[a]	η_Q	J (Hz)[b]	R_{DD} (Hz)[c]	ΔJ (Hz)	β (deg)	α (deg)
$CpCuPEt_3$		19.6(1)	32.2(2)	0.01(1)	2248(53)	1425(50)	0	0	0
$CpCuPPh_3$		28.1(1)	29.4(2)	0.03(1)	2320(10)	1425(40)	0	0	0
$Cp^{\dagger}CuPPh_3$		27.1(6)	25.4(3)	0.07(2)	2323(50)	1457(20)	0	0	0
Cp^*CuPPh_3	site 1	28.9(1)	24.3(2)	0.05(3)	2286(35)	1492(100)	750(320)	0	0
	site 2	28.1(1)	24.3(2)	0.05(3)	2291(12)	1490(90)	750(320)	0	0
$ClCuP(2,4,6)_3$		−65.1(1)	60.6(3)	0.25(1)	2170(25)	1300(100)	750(100)	0	0
$(hfac)CuPMe_3$	site 1	−44.7(2)	−52.5(5)	0.85(5)	2483(22)	1402(55)	750(430)	90	90
	site 2	−43.5(3)	−52.5(5)	0.85(5)	2420(32)	1410(110)	750(430)	90	90
	site 3	−43.5(3)	−52.5(5)	0.85(5)	2420(32)	1408(110)	750(430)	90	90
$[ClCuPPh_2Mes]_2$		−17.0(2)	−51.2(6)	0.50(2)	2080(15)	1325(100)	650(400)	90	90
$[BrCuPPh_2Mes]_2$	site 1	−21.5(2)	−50.2(3)	0.55(2)	2002(35)	1304(300)	650(400)	90	90
	site 2	19.7(2)	−50.2(3)	0.55(2)	1955(40)	1360(400)	650(500)	90	90
$[ICuPPh_2Mes]_2$		−15.8(3)	−46.9(2)	0.48(2)	1780(20)	1262(120)	750(300)	90	90
$[BrCuPPh_3]_4 \cdot 2CHCl_3$	trigonal	−4.7(2)	−51.0(3)	0.39(2)	1938(40)	1309(200)	750(600)	90	90
	tetrahedral	−7.9(1)	23.5(4)	0.79(3)	1959(30)	1288(150)	750(700)	0	0
$[ICuPPh_3]_4$	trigonal	−8.2(1)	−47.5(4)	0.49(2)	1745(43)	1252(214)	750(400)	90	90
	tetrahedral	−15.8(1)	22.0(4)	0.36(2)	1760(20)	1229(150)	750(400)	0	0

[a] On the basis of ^{65}Cu NMR results. [b] J coupling constants are measured directly from the ^{31}P CP/MAS spectra; ^{63}Cu data can be calculated according to the ratio $J(^{31}P,^{65}Cu)/J(^{31}P,^{63}Cu) = 1.0706$. [c] Dipolar coupling constants were calculated from crystallographic values of r_{AB}.

orientation of the dipolar vector with respect to the EFG tensor frame.[49] Since C_Q and η_Q values have been experimentally determined, $^1J(^{65}Cu, ^{31}P)$, $^1J(^{63}Cu, ^{31}P)$, and $\delta_{iso}(^{31}P)$ are directly measured from/between the central peaks of the ^{31}P NMR spectrum, and the magnitude and sign of R_{DD} can be calculated from known r(Cu−P), only four variables remain to fit this spectrum: α^D, β^D, ΔJ, and the sign of C_Q. The sign of $^1J(^{65}Cu, ^{31}P)$ is known to be positive, and hence is not a factor in determining spectral appearance.[49,120] The symmetry of both the molecule and EFG tensor can be used to make accurate predictions of α^D and β^D in most cases herein, leaving the ΔJ and sign of C_Q as the remaining variables. It has been demonstrated by Wasylishen and co-workers that ΔJ can be significant in linear Cu−P bonding environments;[82] hence, this was accounted for in our simulations where possible, with values of $|\Delta J|$ ranging from ca. 600−750 Hz. This indicates that there are additional indirect spin−spin coupling mechanisms at work aside from the usually dominant Fermi contact interaction. Inclusion of values of ΔJ in the range prescribed above as simulation parameters has a relatively minor effect on peak positions (Figure S13); hence, the associated errors in ΔJ are relatively large.

With the exception of the complexes with trigonal planar copper environments, excellent agreement between experimental and simulated data is obtained with $\beta^D \cong 0°$ and $\alpha^D \cong 0°$, indicating that the dipolar vector (Cu−P bond) is along or near the largest component of the EFG tensor, V_{33}. Since these complexes have η_Q values near zero, V_{33} is the distinct component in each case and is oriented along or close to the Cu−P internuclear vector. The trigonal planar compounds, $(hfac)CuPMe_3$, $[XCuPPh_2Mes]_2$, $[BrCuPPh_3]_4 \cdot 2CHCl_3$, and $[ICuPPh_3]_4$, have both β^D and α^D near 90°, indicating that V_{33} is perpendicular to the trigonal planar arrangement of atoms and that V_{22} is along/near the Cu−P bond vector. The sign of C_Q must also be taken into consideration in these simulations: for instance, in the trigonal planar site of $[ICuPPh_3]_4$, if C_Q is taken as positive, then the best fit is achieved with $\beta^D = 45°$ and $\alpha^D = 0°$. This is highly unlikely since it is well-known that quadrupolar nuclei with trigonal planar coordination environments have V_{33} oriented perpendicular to the trigonal plane.[109] With a negative value for C_Q, $\beta^D = \alpha^D = 90°$. It is interesting to note that in all the complexes with V_{33} along or near the Cu−P bond ($\beta^D = 0°$), the signs of C_Q are positive, whereas for the trigonal planar complexes ($\beta^D = 90°$), the signs are negative. Since the nuclear electric quadrupole moments, eQ's, of ^{63}Cu and ^{65}Cu are negative, V_{33} is negative when oriented in a direction of high electron density, and is positive when oriented away from strong bonding MOs.

To summarize, the combination of $^{63/65}$Cu and ^{31}P NMR spectra of Cu−P spin pairs is very useful for determining the orientation of the EFG tensor in the molecular frame as well as the sign of C_Q. Without the $^{63/65}$Cu NMR data, it is possible to make approximations regarding the magnitude of C_Q, though these are subject to significant error. For instance, Olivieri measured residual dipolar coupling constants for a variety of copper(I) phosphines, including $ClCuP(2,4,6)_3$ and the tetrahedral site of $[ICuPPh_3]_4$. $C_Q(^{63}Cu)$ values were estimated to be 69.8 and 30.8 MHz, respectively, which are overestimated by as much as 30%. Hence, some degree of caution must be taken in calculating EFG tensor parameters using these challenging multiparameter simulations.

Theoretical Calculations of $^{65/63}$Cu EFG Tensors. Ab initio calculations were performed on all compounds, employing various methods and basis sets, to examine the relationships between EFG tensor components and orientations, and molecular structure and symmetry, and to confirm our predictions from experimental data. The best agreements between experimental and theoretical values are observed for RHF calculations with 6-31++G** and 6-311G** basis sets (Table 5); in particular, the 6-31++G** calculations are remarkably close to experimental results, and hence, are the focus of the remainder of discussion in this section. No improvements in agreement with experimental data were noted for larger basis set sizes, or from using DFT methodologies (see Tables S6 to S14 for a complete listing of calculations).

Calculations on $[Cu(PhCN)_4]BF_4$ were performed on only the $(PhCN)_4Cu^+$ cation. Because of the relatively high symmetry of this copper environment compared to other complexes discussed herein, a large variability in calculated C_Q values is observed as a function of basis set, with larger Huzinaga basis sets[92] producing more consistent sets of values. The EFG tensor components are not aligned with Cu−N bonds or any distinct

(120) Menger, E. M.; Veeman, W. S. *J. Magn. Res.* **1982**, *46*, 257.

Table 5. Theoretical Gaussian03 EFG Calculations Using the RHF Method

basis set	V_{11} (au)[a]	V_{22} (au)	V_{33} (au)	C_Q (^{63}Cu) (MHz)[b,c,d]	C_Q (^{65}Cu) (MHz)[b,d]	η_Q
			$(PhCN)_4Cu^+$			
experimental				**+4.10(10)**	**3.63(10)**	**0.95(5)**
6-311G**	0.0309	0.0865	−0.1174	+6.07	+5.63	0.47
6-31++G**	0.0146	0.0654	−0.0800	+4.14	+3.83	0.64
			$CpCuPEt_3$			
experimental				**+34.7(3)**	**+32.2(2)**	**0.01(1)**
6-311G**	−0.3255	−0.4060	0.7316	−37.82	−35.07	0.11
6-31++G**	−0.2958	−0.3678	0.6636	−34.30	−31.81	0.11
			$CpCuPPh_3$			
experimental				**+31.7(3)**	**+29.4(2)**	**0.03(1)**
6-311G**	−0.3936	−0.4217	0.8153	−42.14	−39.08	0.03
6-31++G**	−0.2852	−0.3152	0.6003	−31.03	−28.78	0.05
			$Cp^\dagger CuPPh_3$			
experimental				**+27.4(4)**	**+25.4(3)**	**0.07(2)**
6-311G**	−0.3218	−0.4265	0.7483	−38.68	−35.87	0.140
6-31++G**	−0.2336	−0.3091	0.5427	−28.05	−26.01	0.139
			Cp^*CuPPh_3			
experimental				**+26.2(3)**	**+24.3(2)**	**0.05(3)**
6-311G**	−0.3713	−0.4185	0.7898	−40.83	−37.86	0.06
6-31++G**	−0.2486	−0.2961	0.5448	−28.16	−26.11	0.09
			$ClCuP(2,4,6)_3$			
experimental					**+60.6(3)**	**0.25(1)**
6-311G**	−0.5081	−0.8007	1.3088	−67.66	−62.73	0.22
6-31++G**	−0.5394	−0.7434	1.2828	−66.31	−61.49	0.16
			*(*hfac)$CuPMe_3$			
experimental					**−52.5(5)**	**0.90(5)**
6-311G**	0.3477	1.0260	−1.3736	+71.01	+65.84	0.49
6-31++G**	0.1086	0.9864	−1.0950	+56.60	+52.49	0.80
			$Me_3NNCuCNAr$			
experimental					**71.0(1)**	**0.11(1)**
6-311G**	0.9013	1.0671	−1.9683	+101.75	+94.35	0.08
6-31++G**	0.6311	0.8500	−1.4811	+76.56	+71.00	0.15
			$[ClCuPPh_2Mes]_2$			
experimental					**−51.2(6)**	**0.50(2)**
6-311G**	0.2741	0.9478	−1.2218	+63.15	+58.56	0.55
6-31++G**	0.2530	0.8237	−1.0767	+55.66	+51.61	0.530
			$[BrCuPPh_2Mes]_2$			
experimental					**−50.2(3)**	**0.55(2)**
6-311G**	0.2543	0.9514	−1.2060	+62.33	+57.79	0.578
6-31++G**	0.2636	0.7862	−1.0498	+54.27	+50.32	0.498
			$[ICuPPh_2Mes]_2$[e]			
experimental					**−46.9(2)**	**0.48(2)**
6-311G**	0.3348	0.8752	−1.2100	+62.55	+58.00	0.447
	0.2742	0.8745	−1.1488	+59.38	+55.06	0.523
6-31++G**	0.2647	0.7455	−1.0103	+52.22	+48.43	0.476
	0.2348	0.7324	−0.9672	+50.00	+46.36	0.515
			$[BrCuPPh_3]_4 \cdot 2CHCl_3$			
	tetrahedral copper site					
experimental					**+23.5(4)**	**0.79(3)**
6-311G**	−0.1160	−0.4618	0.5778	−29.87	−27.70	0.599
6-31++G**	−0.1334	−0.4170	0.5503	−28.45	−26.38	0.515
	trigonal copper site					
experimental					**−51.0(3)**	**0.39(2)**
6-311G**	0.3596	0.8836	−1.2432	+64.27	+59.59	0.422
6-31++G**	0.2929	0.7899	−1.0828	+55.97	+51.90	0.459
			$[ICuPPh_3]_4$[f]			
	tetrahedral copper site					
experimental					**+22.0(4)**	**0.36(2)**
6-311G**	−0.1023	−0.4067	0.5090	−26.31	−24.40	0.60
6-31++G**	−0.1336	−0.3440	0.4777	−24.69	−22.90	0.44
	trigonal copper site					
experimental					**−47.5(4)**	**0.49(2)**
6-311G**	0.3588	0.8460	−1.2048	+62.28	+57.75	0.40
6-31++G**	0.2958	0.7261	−1.0219	+52.82	+48.98	0.42

[a] V_{ii} are the principal components of the EFG tensor, where $|V_{33}| \geq |V_{22}| \geq |V_{11}|$. [b] Calculated C_Q is converted from atomic units into Hz by multiplying V_{33} by $(eQ/h)(9.7177 \times 10^{21}\ \mathrm{V\ m^{-2}})$, where $Q(^{65}\mathrm{Cu}) = -0.220 \times 10^{-28}\ \mathrm{m^2}$, $Q(^{65}\mathrm{Cu}) = -0.204 \times 10^{-28}\ \mathrm{m^2}$ and $e = 1.602 \times 10^{-19}$ C.[124] [c] The signs from G03 are being reported even though they are opposite on the basis of the conventions mentioned in the text. [d] C_Q values without a + or − sign indicates absolute values are reported. [e] The 3-21G** was used on I atoms and the given basis sets in the table were used on all other atoms. [f] For the I atoms and for the C and H atoms, basis sets 3-21G** and 6-31G** were used, respectively, and remained constant for all calculations. Basis sets for Cu and P are those given in the table.

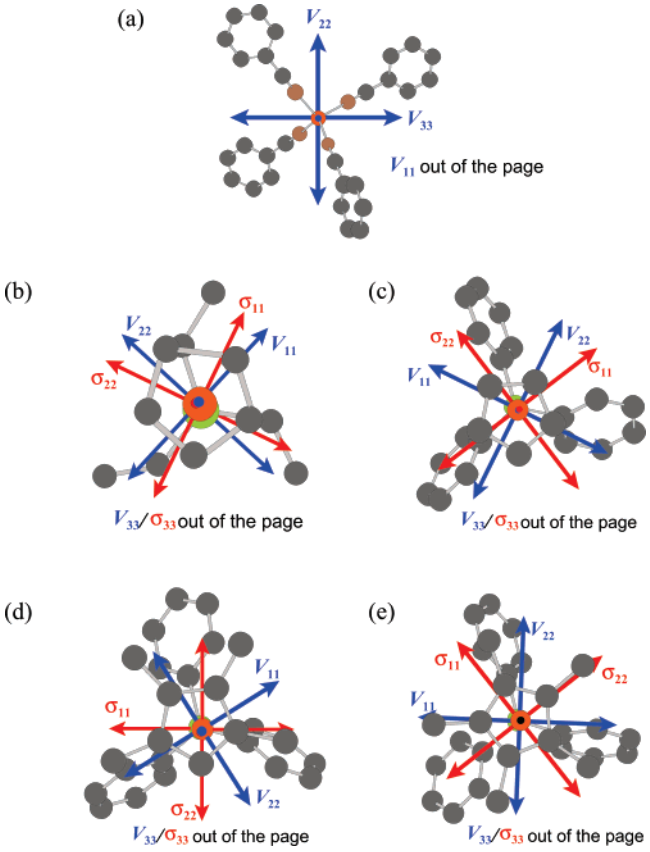

Figure 10. ^{65}Cu EFG tensor orientation for (a) $[(PhCN)_4Cu]^+$ and EFG and CS tensor orientation for (b) $CpCuPEt_3$, (c) $CpCuPPh_3$, (d) $Cp^{\dagger}CuPPh_3$, and (e) Cp^*CuPPh_3. All orientations are from RHF/6-31++G** calculations. Protons were removed for clarity.

symmetry elements (Figure 10a), owing to the relatively distorted tetrahedral environment. This accounts for the larger C_Q in comparison to highly tetrahedral Cu environments[6] as well as the nonzero value of η_Q.

Calculations of C_Q and η_Q for the Cp′CuPR$_3$ compounds are in close agreement with experimental results, though the values of C_Q for Cp^*CuPPh_3 and $Cp^{\dagger}CuPPh_3$ are predicted to be almost the same. Theoretical tensor orientations match well with predictions from our ^{31}P NMR experiments, with V_{33} along or very near to the Cu−P bonds, and therefore toward the centroids of the Cp′ rings (Figure 10b−e). V_{11} and V_{22} are oriented in nearly identical electronic environments, accounting for the axial symmetry of the EFG tensors ($\eta_Q \approx 0$). The orientation of V_{33} toward the P−Cu−Cp$_{cent}$ direction makes sense, given that the largest potential differences and field gradients are along this direction, owing to both the high electron density in the Cp′ rings (Figure S14) and the strong covalent character of the Cu−P bonds.

In ClCuP(2,4,6)$_3$ (Figure 11a), V_{33} is the distinct component and is directed near the pseudo-3-fold axis with a V_{33}−Cu−Cl angle of 3.03°. This slight tilt differentiates V_{11} and V_{22}, giving rise to a nonzero η_Q. The C_Q is significantly larger in this complex than in the metallocenes, undoubtedly because of the increase in the Cu−P bond distance and the presence of the Cl atom along the pseudo-3-fold axis. For both (hfac)CuPMe$_3$ and [Me$_3$NN]Cu(CNAr), V_{33} is oriented perpendicular to the trigonal plane (Figure 11b,c), consistent with previous theoretical observations in a number of trigonal planar systems.[63,109,115] This agrees with our experimental prediction of the EFG tensor orientation from the ^{31}P NMR spectra of (hfac)CuPMe$_3$, with V_{22} oriented very close to the Cu−P bond ($(\angle P-Cu-V_{22}) = 3.93°$). Unfortunately, *J*-coupling and/or residual dipolar couplings between ^{13}C and $^{63/65}$Cu in [Me$_3$NN]Cu(CNAr) could not be clearly resolved in the ^{13}C CP/MAS NMR spectrum (Figure S3), so no experimental copper tensor orientation is available for this molecule. The different η_Q values arise from the extremely different bonding environments around the copper atom. Mulliken population analysis for (hfac)CuPMe$_3$ (Figure 12a), indicates that there is a high amount of electron density within the hfac substituent, and a low amount of electron density in the phosphine region, which results in a fairly large electric field gradient component along this direction. Since there are large, similar EFG contributions both perpendicular to the trigonal plane and along the Cu−P bond, the η_Q value is close to 1, with V_{11} as the distinct component. In contrast, electron density and corresponding field gradients in the trigonal plane about the copper atom of [Me$_3$NN]Cu(CNAr) are quite uniform, giving rise to similar values of V_{11} and V_{22} (Figure 12b).

For the [XCuPPh$_2$Mes]$_2$ compounds, V_{33} is oriented perpendicular to the trigonal plane (Figure 11d−f), and V_{22} is oriented very close to the Cu−P bond vectors (with ($\angle$P−Cu-V_{22}) between 1.70° and 7.16°). The reasoning for the nonzero η_Q follows a similar argument as that for (hfac)CuPMe$_3$ (Figure 12c−e). Very similar results were obtained for the trigonal copper sites of [XCuPPh$_3$]$_4$ and are also in good agreement with predictions from ^{31}P NMR spectra (Figure 11g,h). For the tetrahedral sites of [XCuPPh$_3$]$_4$, V_{33} points in the same direction as the shortest Cu−P bond.

Finally, some comments should be made on the signs of the EFG tensor components calculated using the Gaussian 03 software package. The predicted signs of C_Q from the G03 calculations are opposite to those determined experimentally in nearly every case (Table 5). This discrepancy is not believed to arise from any sort of simulation or calculation errors, but rather, from the sign conventions for the electron density utilized in the calculation of V_{33} in Gaussian 03.[121,122] This inconsistency is described in more detail in the Supporting Information.

Theoretical Calculations of Copper CS Tensors. Although copper CSA was only observed for a few compounds, calculations were conducted on all structures (Table 6), and a very brief discussion is presented here. Calculations on the Cp′CuPR$_3$ complexes are in good agreement with the experimental values for both the Ω and κ. The most shielded component, σ_{33}, is coincident with V_{33} for all complexes (Figure 10b−e), while σ_{11} and σ_{22} are oriented in similar environments, yielding values of κ near 1. Calculations on the trigonal planar phosphorus environments in the [XCuPPh$_2$Mes]$_2$ series yield very good agreement for values of Ω, though values of κ are not accurately predicted. Nonetheless, the predicted CS tensor orientations are in very good agreement with our experimental data, with σ_{11} consistently oriented perpendicular to the trigonal plane (Figure 11d−f). CSA contributions to the copper powder patterns of

(121) Wu, X.; Fronczek, F. R.; Butler, L. G. *Inorg. Chem.* **1994**, *33*, 1363.
(122) Bryce, D. L.; Gee, M.; Wasylishen, R. E. *J. Phys. Chem. A* **2001**, *105*, 10413.
(123) Mulla-Osman, S.; Michel, D.; Volkel, G.; Peral, I.; Madariaga, G. *J. Phys.: Condens. Matter* **2001**, *13*, 1119.
(124) Coriani, S.; Hattig, C.; Jorgensen, P.; Rizzo, A.; Ruud, K. *J. Chem. Phys.* **1998**, *109*, 7176.

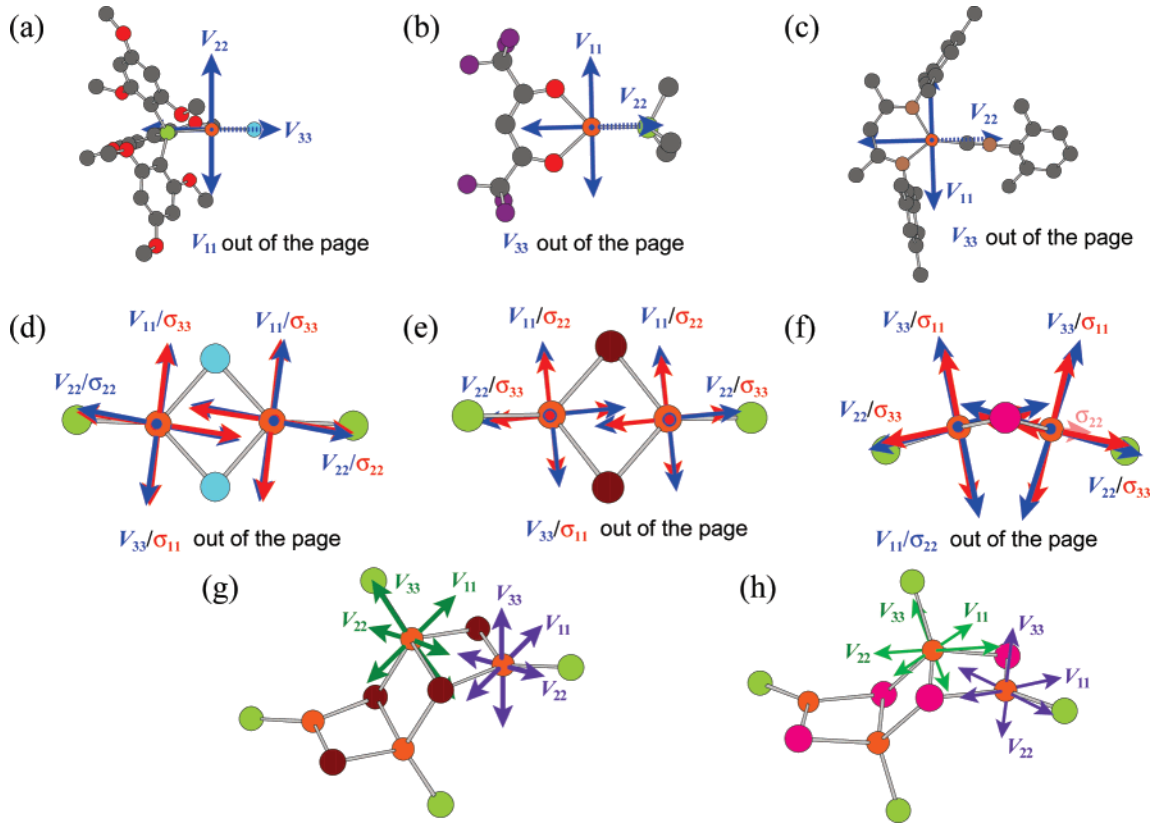

Figure 11. ^{65}Cu tensor orientations for (a) $ClCuP(2,4,6)_3$, (b) $(hfac)CuPMe_3$, (c) $[Me_3NN]Cu(CNAr)$, (d) $[ClCuPPh_2Mes]_2$, (e) $[BrCuPPh_2Mes]_2$, (f) $[ICuPPh_2Mes]_2$, (g) $[BrCuPPh_3]_4{\cdot}2CHCl_3$, and (h) $[ICuPPh_3]_4$. Dashed vectors denote tensors along the bond. All orientations are from RHF/6-31++G** calculations. Protons, phosphines, and mesityl groups are removed for clarity.

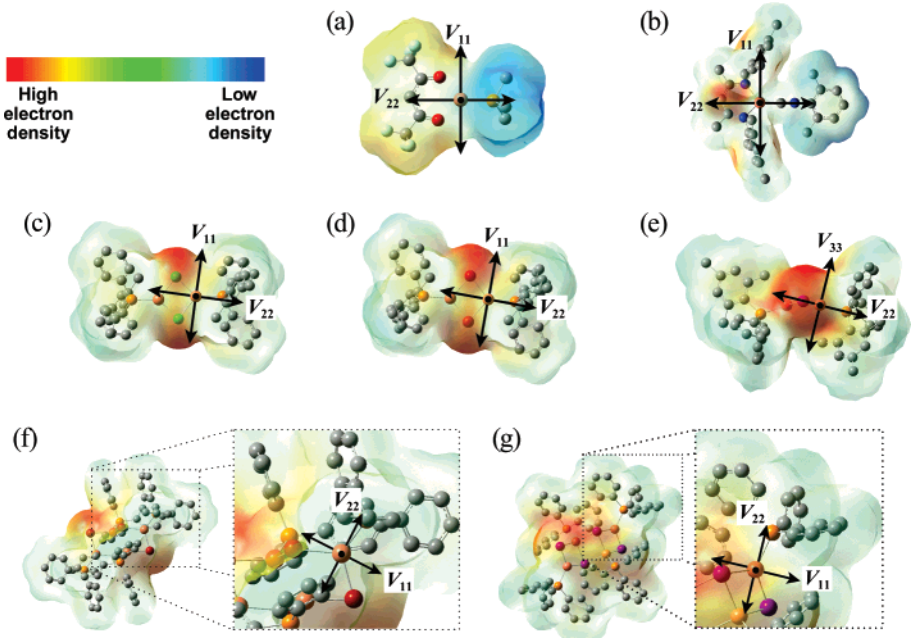

Figure 12. Correlation of electron density and EFG tensor orientations of (a) $(hfac)CuPMe_3$, (b) $[Me_3NN]Cu(CNAr)$, (c) $[ClCuPPh_2Mes]_2$, (d) $[BrCuPPh_2Mes]_2$, (e) $[ICuPPh_2Mes]_2$, (f) $[BrCuPPh_3]_4{\cdot}2CHCl_3$, and (g) $[ICuPPh_3]_4$. In all cases, V_{33} components are perpendicular to the page.

$ClCuP(2,4,6)_3$, $(hfac)CuPMe_3$, and $[Me_3NN]Cu(CNAr)$ were not taken into account when simulating these powder patterns because the effect is believed to be insignificant. The predicted spans (Tables S22 and S23) are not expected to have any noticeable effect on the total breadth of the copper powder patterns; for example, with total pattern breadths between ca. 5.0 and 6.5 MHz, a span of 2000 ppm (with $\kappa = 1.0$) only results in a 3% increase in breadth (Figure S8).

Conclusion

Piecewise frequency-stepped QCPMG NMR experiments have been successfully used to acquire ^{65}Cu and ^{63}Cu NMR

Table 6. Theoretical Gaussian03 Copper CS Tensor Calculations Using RHF and B3LYP Methods

method		δ_{11} (ppm)	δ_{22} (ppm)	δ_{33} (ppm)	δ_{iso} (ppm)[a]	Ω (ppm)[b]	κ[c]
				$CpCuPEt_3$			
experimental					**−50(6)**	**1300(300)**	**0.95(5)**
RHF/6-31++G**		1120.15	1046.32	−223.98	647.50	1344.13	0.890
RHF/6-311G**		838.56	767.67	−478.34	375.96	1316.90	0.892
B3LYP/6-31++G**		980.43	875.80	−464.21	464.01	1444.65	0.855
B3LYP/6-311G**		−605.60	−723.20	−2109.64	−1146.15	1504.04	0.844
				$CpCuPPh_3$			
experimental					**−30(40)**	**1500(250)**	**0.90(10)**
RHF/6-31++G**		1120.79	1080.47	−217.38	661.29	1338.17	0.940
RHF/6-311G**		994.30	919.84	−454.39	486.58	1448.69	0.897
B3LYP/6-31++G**		994.28	928.95	−425.77	499.15	1420.06	0.908
B3LYP/6-311G**		−415.83	−543.22	−2052.87	−1003.97	1637.04	0.844
				$Cp^{\dagger}CuPPh_3$			
experimental					**0(80)**	**1300(200)**	**0.95(5)**
RHF/6-31++G**		1124.42	1086.49	−130.58	693.44	1255.00	0.940
RHF/6-311G**		969.27	885.73	−383.24	490.59	1352.51	0.876
B3LYP/6-31++G**		997.38	918.97	−317.99	532.79	1315.38	0.881
B3LYP/6-311G**		−457.50	−572.14	−1922.15	−983.93	1464.65	0.843
				Cp^*CuPPh_3			
experimental					**−50(50)**	**1200(200)**	**0.95(5)**
RHF/6-31++G**		1140.64	1105.65	−108.03	712.75	1248.67	0.944
RHF/6-311G**		982.21	926.25	−349.66	519.60	1331.87	0.916
B3LYP/6-31++G**		986.68	930.27	−292.74	541.40	1279.42	0.912
B3LYP/6-311G**		−452.10	−526.56	−1879.57	−952.75	1427.46	0.896
				$[ClCuPPh_2Mes]_2$			
experimental					**100(200)**	**1100(400)**	**−0.70(20)**
RHF/6-31++G**		1157.58	616.38	140.92	638.29	1016.66	−0.065
RHF/6-311G**		826.64	311.88	−183.90	318.21	1010.54	−0.019
B3LYP/6-31++G**		1339.48	633.38	12.71	661.85	1326.77	−0.064
B3LYP/6-311G**		−295.24	−887.22	−1734.40	−972.29	1439.16	0.177
				$[BrCuPPh_2Mes]_2$			
experimental					**200(250)**	**1000(700)**	**−0.90(10)**
RHF/6-31++G**		1180.90	566.99	186.20	644.70	994.70	−0.234
RHF/6-311G**		905.32	255.19	−158.14	334.12	1063.46	−0.223
B3LYP/6-31++G**		1396.53	579.81	82.24	686.19	1314.29	−0.243
B3LYP/6-311G**		−179.50	−980.24	−1704.58	−954.77	1525.08	−0.050
				$[ICuPPh_2Mes]_2$[d]			
experimental					**100(100)**	**1100(500)**	**−0.90(10)**
RHF/6-31++G**	site 1	1358.76	548.05	412.60	773.14	946.16	−0.714
	site 2	1377.31	528.11	392.61	766.01	984.70	−0.725
RHF/6-311G**	site 1	1117.37	223.12	10.03	450.17	1107.34	−0.615
	site 2	1123.75	191.14	−0.06	438.28	1123.81	−0.660
B3LYP/6-31++G**	site 1	100.48	−1062.76	−1424.16	−795.48	1524.64	−0.526
	site 2	117.40	−1125.40	−1469.28	−825.76	1586.68	−0.567
B3LYP/6-311G**	site 1	1513.23	520.45	350.89	794.85	1162.35	−0.708
	site 2	1569.17	490.21	329.31	796.23	1239.86	−0.740

[a] Isotropic shift, $\delta_{iso} = (\delta_{11} + \delta_{22} + \delta_{33})/3$. [b] Span of the CS tensor, $\Omega = \delta_{11} - \delta_{33}$. [c] Skew of the CS tensor, $\kappa = 3(\delta_{22} - \delta_{iso})/\Omega$. [d] The 3-21G** was used on I atoms and basis sets given in the table were used on all other atoms.

spectra of complexes with extremely large copper quadrupolar interactions. These spectra provide information on copper quadrupolar parameters and chemical shifts for a series of copper environments for which solid-state NMR spectra have never been acquired. Residual dipolar coupling in the ^{31}P NMR spectra of complexes with Cu−P spins pairs enable the determination of the sign of C_Q as well as the orientation of the Cu−P vectors with respect to the EFG tensor frames. Ab initio calculations, using RHF/6-31++G** and RHF/6-311G**, were extremely successful in predicting both EFG tensor parameters and their orientations. We believe that this work demonstrates that solid-state wide-line $^{63/65}Cu$ NMR spectroscopy holds much promise for the structural characterization of spherically asymmetric Cu(I) sites in a variety of systems of scientific and technological importance, including biological Cu complexes and assorted mesoporous and microporous materials.

Acknowledgment. The Natural Sciences and Engineering Research Council (NSERC, Canada), the Canadian Foundation for Innovation (CFI), and the Ontario Innovation Trust (OIT) are gratefully acknowledged for financial support. R.W.S. and J.A.T. acknowledge the Centre for Catalysis and Materials Research (CCMR) at the University of Windsor, Imperial Oil, and NSERC CRD for additional funding. T.H.W. is grateful to the NSF CAREER program (Grant CHE-01350507) for support of this work. We would like to thank Yosra M. Badiei (Georgetown University) for providing the sample of $[Me_3NN]$-Cu(CNAr). We are grateful to Prof. Alex Bain (McMaster University) for assistance in simulations of $^{63/65}Cu$ NMR powder patterns with large quadrupolar coupling constants. We thank Dr. Victor Terskikh and Dr. Shane Pawsey for assistance in acquiring copper NMR data at the National Ultrahigh-field NMR Facility for Solids in Ottawa (http://www.nmr900.ca) and Dr.

Andy Lo for assistance with low-field data acquisition. We would also like to thank Prof. Jochen Austchbach (SUNY Buffalo) for helpful discussions and Mr. Sinisa Jezdic for assistance with probe modifications.

Supporting Information Available: Complete refs 23, 24, 88, and 89; X-ray crystallographic data for $Cp^{\dagger}CuPPh_3$ and Cp^*CuPPh_3; sample preparation; powder X-ray diffraction patterns; additional $^{63/65}Cu$, ^{31}P, and ^{13}C NMR data; additional EFG and CS tensor calculations; tensor coordinates; energies for ab initio/DFT calculations; CIF files for $CpCuPEt_3$, $Cp^{\dagger}CuPPh_3$, and Cp^*CuPPh_3. This material is available free of charge via the Internet at http://pubs.acs.org.

JA073238X